

Erasmus MC

# Parameter verification of a hybrid MRI Hyperthermia applicator

Peter Baronner

07-06-2013

The research that is described in this paper was performed at the Daniel den Hoed Kliniek, which is part of the Erasmus university of Rotterdam. During my research I have been coached by Wouter Numan. I would like to thank him for all the support he has offered. Also, I would like to thank Ruben Pellicer, for his assistance in fabricating the phantoms. I have enjoyed the time I was given there.

## Abstract

Cancer is a worldwide human health problem. This is why much effort is put in finding solutions and treatments for this disease. One of the emerging adjuvant cancer treatments, hyperthermia, is applied by heating the tumour tissue, and is shown to increase the effects of radio and/ or chemotherapy.

Because of the difficulty in the controlled heating inside the head and neck region, the MRIlabcollar applicator has been designed. This applicator uses twelve antennae to heat specific parts of tissue, and can be used inside the MRI, since the use of Ferro-magnetic materials was minimised. This way, the temperature distribution can be visualised during the measurement.

In order to simulate the measurements of the MRIlabcollar, some parameters need to be verified. first, an experimental phantom was fabricated, which the human neck for its dielectric properties. The antenna impedance, as well as its sensitivity to changes in the phantom, temperature and input power were measured. Also, the coupling between the antennae was measured.

The antenna's impedance showed no significant reaction due to the changes in the phantom material. The temperature however affected the resonance frequency, and thus the impedance of the antenna. In order for the antennae to resonate at 434 MHz, which is a frequency reserved for scientific experiments, the optimal temperature is somewhere between 30 and 35 °C.

This was further shown during the power measurements. When power was increased, the temperature, and thus the return loss of the antennae increased.

The total coupling of the antennae at 434 MHz was found to be between -8 and -9dB. The coupling between individual antennae is measured on -16dB.

During the measurements we found that antenna 1\_2 shows variance in its return loss when its cable is moved, an effect not seen by the other antennae. This might indicate the antenna or connector is of unsound construction.

# Content

Abstract.....	2
1. Introduction to hyperthermia.....	5
1.2 Head and neck hyperthermia .....	5
1.3 Thermometry and MRT .....	5
1.4 Experimental HT and MRT .....	5
1.5 Verification and validation.....	6
2. Background.....	7
2.1 The patch antenna.....	7
2.2 S-parameters .....	8
3. Method .....	9
3.1 Construction of a fat and muscle equivalent phantom .....	9
3.2 Antenna base impedance.....	11
3.3 Sensitivity of the antenna impedance.....	11
3.3.1 Sensitivity to temperature and phantom material changes.....	12
3.3.2 Sensitivity to input power .....	12
3.4 Coupling measurements.....	12
4. Results and discussion .....	13
4.1 Dielectric properties of the phantom.....	13
4.2 Antenna base impedance.....	15
4.3 Sensitivity of the antenna impedance.....	16
4.3.1 Phantom sensitivity .....	16
4.3.2 Temperature sensitivity.....	17
4.3.3 Power sensitivity .....	18
4.4 Coupling measurements.....	21
Conclusion .....	23
References .....	24
Appendix I: Fabrication of a fat and muscle equivalent phantom.....	25
Muscle equivalent material .....	25
Fat equivalent material .....	25
Appendix II: VNA and dielectric measurement kit .....	26
Appendix III: Power measurement setup .....	27
Appendix IV: Results .....	28
$S_{11}$ measurements .....	28
$S_{21}$ measurements, Graphs .....	34
$S_{21}$ measurements, values at 434 MHz.....	40
Antenna 1_2 .....	42

Time dependency of the dielectric measurement kit and the VNA .....	44
Appendix V: The original assignment.....	45

## 1. Introduction to hyperthermia

Cancer is a worldwide human health problem. Around 13% of all human deaths (7.9 million in 2008) are a direct result of tumours<sup>9</sup>. Because of the increasing health care, especially in Europe, the rates are even rising, as people live to older ages and lifestyle changes occur in the developing parts of the world<sup>1</sup>. The treatment for cancer patients usually consists of chemo and radio therapy, sometimes in combination with surgery. Hyperthermia (HT) is an emerging adjuvant cancer treatment modality, which is at the centre of scientific interest. Treatment is applied by raising tumour temperatures, using interference patterns of electromagnetic waves (EM-waves, to around 40-42 °C for about an hour.) While hyperthermia itself is not very likely to kill cells at those temperatures<sup>2</sup>, several studies have demonstrated the efficacy of the addition of this hyperthermia treatment when applied after radio or chemotherapy.

### 1.2 Head and neck hyperthermia

Applying HT at the head and neck (H&N) region comes with its own challenges. The head and neck region consists of widely varied tissues with different effects on EM-wave distribution and cooling. Accurately modelling and effective application of heating in these regions requires innovative new technologies.

### 1.3 Thermometry and MRT

One of the challenges in hyperthermia is offered by the wish to accurately monitor the temperature throughout the tumour, a process currently performed by special probes inserted into the patient. These probes are very thin optical wires with multiple thermometers. Using these probes is an invasive technique, which can lead to patient discomfort, or even harm. Therefore it is worth the effort to study non-invasive temperature measurement, such as MRI Thermometry(MRT). This technique can be used to make a 3D temperature map using Magnetic Resonance Imaging (MRI).

### 1.4 Experimental HT and MRT

To test combined HT and MRT, a low distortion applicator, called the MRlabcollar, was designed with reduced metal surfaces and non-ferrous materials, and the option to quickly exchange target phantoms. As seen in figure 1.1, the MRlabcollar applicator is a cylindrical device with two compartments. The inner compartment is empty, and can be filled with a human tissue mimicking phantom. The outer compartment has 2 rings of 6 antennae attached to it, which emit electromagnetic waves (EM-waves) at a frequency of 433.92 MHz. This is the centre of the frequency range allocated for Industry, Science and Medicine (ISM-frequency) and is a suitable frequency for heating H&N tumours with a multi antenna applicator<sup>7</sup>. The outer compartment is filled with demineralised water, to guide the electromagnetic waves into the phantom without too much boundary reflections, and to cool the antennae and patient surface.

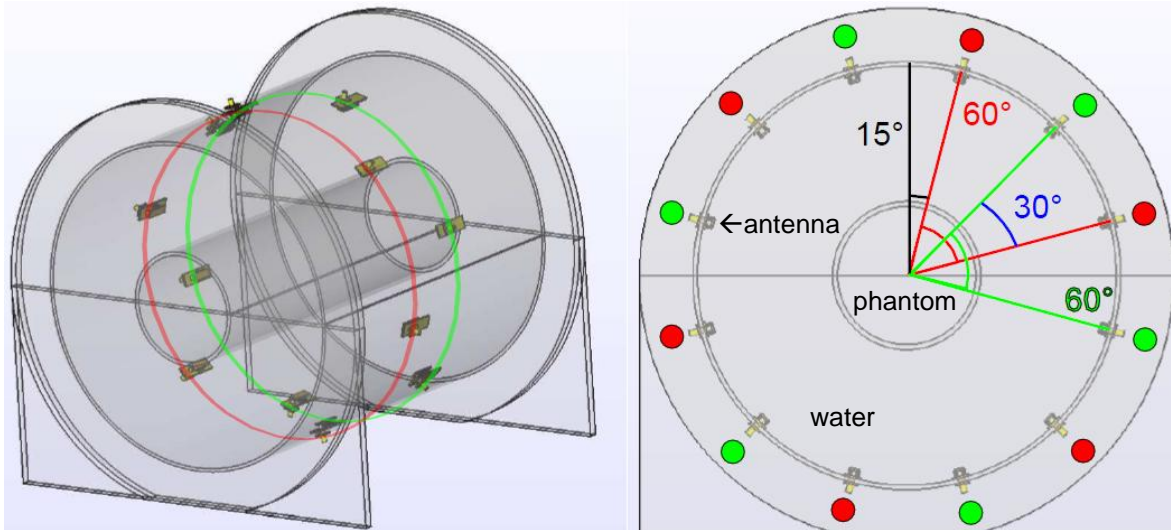


Figure 1.1; the MRlabcollar; The 12 antennae are divided into two rings, 80 mm apart, and have a relative rotation of 30 degrees. Its total length is 450 mm, the diameter of the inner cylinder is 150 mm, the diameter of the outer cylinder is 300 mm. The inner cylinder is empty and is used for the phantom, while the outer cylinder can be filled with water.

### 1.5 Verification and validation

The goal of this study is the characterization of the antenna properties of the MRlabcollar. This needs to be done in order to verify the input parameters used for EM simulations, so that the MRlabcollar can be validated through field comparison with simulation results. This validation is necessary to improving the predictions in preparation of analysing the MRI-thermometry measurements.

## 2. Background

This chapter includes some additional theory about the antennae used for the MRlabcollar, and introduces the *S-parameters*.

### 2.1 The patch antenna

The twelve antennae used inside the applicator are patch antennae. Patch antennae consists of two metal plates, at a certain distance from each other (see figure 2.1 and 2.2). When a high frequency alternating current (AC) is fed to the top patch, the antenna acts like a capacitor. When this frequency becomes high enough, half of the wavelength of the current becomes equal to the length of the top patch. At this frequency, called the resonance frequency or  $f_{res}$ , the phase of the current at the left side of the top patch is exactly opposite to the phase at the right side of the antenna. This resonance is followed by a counter current across the ground plane, resulting in an changing electric and magnetic field between the top and bottom patch of the antenna, as seen in figure 2.3. In a previous study<sup>7</sup>, the antenna dimensions have been designed to resonate at the earlier mentioned 434 MHz.

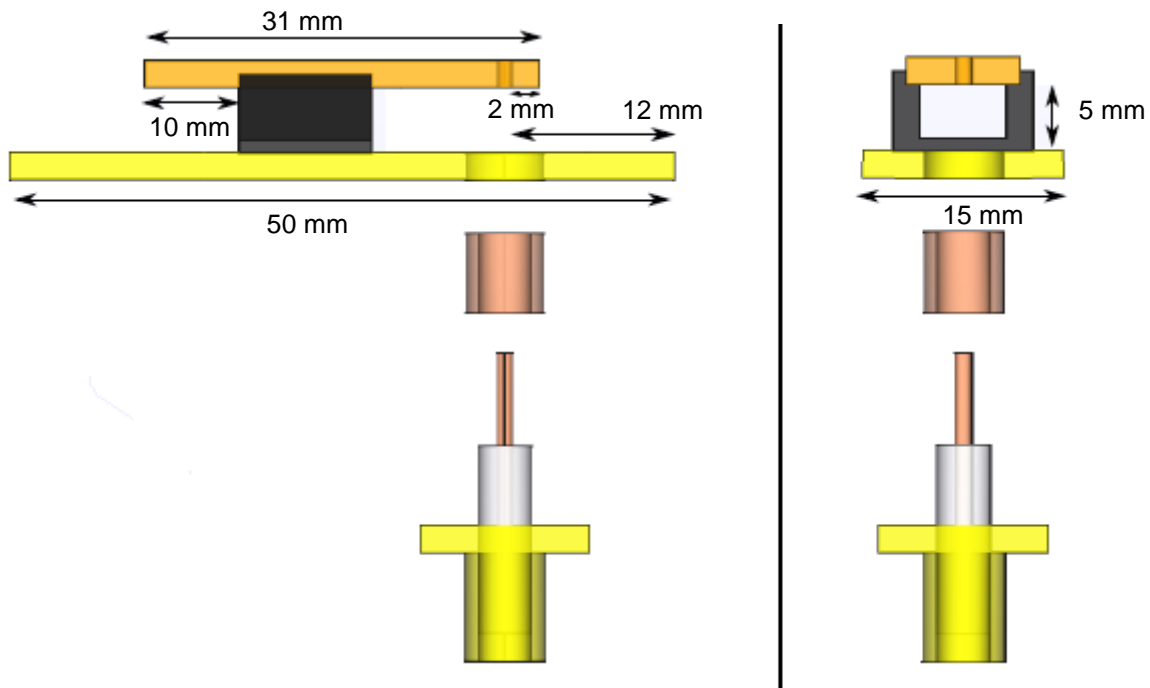


Figure 2.1 and 2.2; the side and front view of the antenna. The orange coloured top patch is fed an high frequency AC.

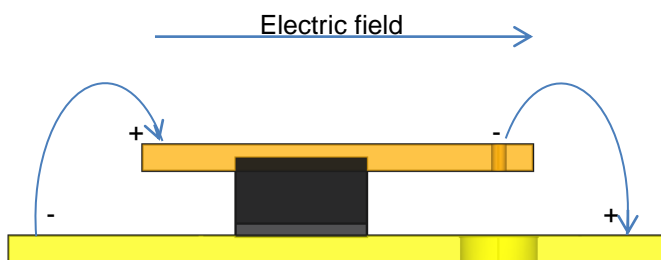


Figure 2.3; at the  $f_{res}$ , the left and right side of the top patch are  $180^\circ$  out phase, resulting in an electric field.

When the antenna is surrounded by any material, the speed of the wave inside the antenna decreases, as a result of the material resisting to the created field. In order for the antenna to keep resonating, the wavelength has to remain the same. Using equation 2.1 we find that, if the wavelength

remains the same, but the speed of the wave decreases, the  $f_{res}$  increases. To compensate for this change in  $f_{res}$ , the antennae length can also be modified.

$$c = \lambda \cdot f_{res} \quad (2.1)$$

In which:

- $c$ : the speed of the wave in meters per second;
- $\lambda$ : the length of the wavel in meters.

The reason for choosing patch antennae over dipole antennae, which are used in most Deep hyperthermia (DHT) applicators<sup>11</sup>, is the fact that these patch antennae can be connected using a simple coax cable, while the dipole antennae require a RF-matching network containing a balun in order to obtain a symmetric radiation field and stable electrical performance<sup>10</sup>. This matching device decreases the efficiency of the antenna.

## 2.2 S-parameters

The scattering parameters (S-parameters) describe the electrical behaviour of networks when receiving electrical signals of varying frequencies. These complex values can be used to show how much of the offered power reflects back to the source, or is picked up by other sources. In a two port system, four S-parameters can be measured, as is shown in figure 2.4. The  $S_{11}$  and  $S_{22}$  represent the reflected power at port one and two respectively, while the  $S_{21}$  and  $S_{12}$  represent the forward and reverse gain of a 2-port system.

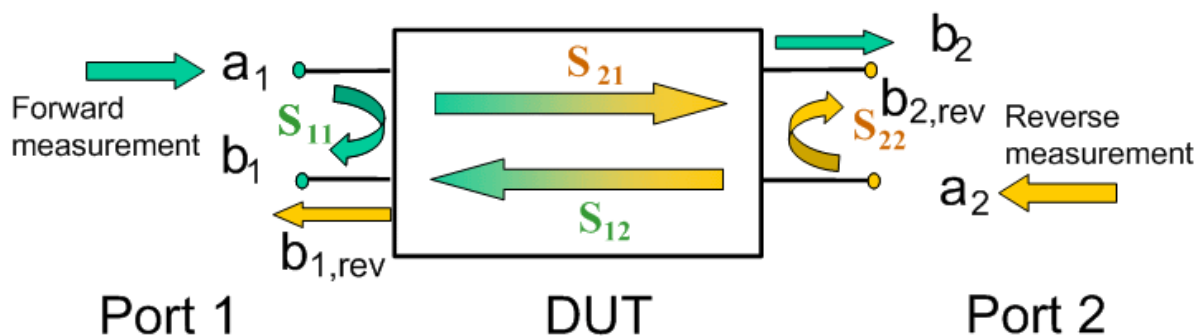


Figure 2.4; the S-parameters of a 2-port system.

When displayed in dB,  $S_{11}$  is named return loss (RL) and  $S_{21}$  the forward transmission coefficient (FTC). These values can be given for current or voltage, or for power, in which case the  $S_{11}$  and  $S_{21}$  are given squared.

The  $S_{11}$ -parameter of the antenna can be used to calculate the antenna's impedance using:

$$Z = Z_0 \cdot \left( \frac{1+S_{11}}{1-S_{11}} \right) \quad (2.2)$$

in which  $Z_0$  is the system's characteristic impedance, which is usually 50  $\Omega$ . The efficiency of the power transfer to the antenna increases when the absolute antenna impedance better matches the feeding systems characteristic impedance.

The FTC, or coupling between the antennae describes how much the antennae influence each other. When the coupled power increases, the measured RL increases as well, therefore giving a false value, affecting the power control.

### 3. Method

SEMCAD X is a 3D full-wave electromagnetic and thermal simulation platform based on the Finite-Difference Time-Domain (FDTD) technique. This technique is used for calculating the behaviour of electromagnetic waves or thermal distributions inside largely inhomogeneous structures, such as a model of the H&N region. Using this program, simulations of the MRlabcollar have been made, to be able to predict the behaviour of the antennae and their heating properties. In order to perform an accurate simulation, the input parameters, such as the antennae impedance or the dielectric properties of the used materials, need to be verified. When the simulation gives results which, within a certain range, agree with measurement results, the simulation is validated.

Simulations used to predict electromagnetically induced hyperthermia make use of the specific absorption rate ( $SAR$  [W/kg]), which is the standard quantity for measuring electromagnetic power absorption in biological tissue.  $SAR$  is calculated using equation:

$$SAR = \frac{\sigma_{eff}|E|^2}{2\rho} \quad (3.1)$$

in which  $E$  is the spatial electric field vector in V/m,  $\rho$  is the mass density of the body in  $\text{kg/m}^3$  and  $\sigma_{eff}$  is the effective conductivity of the material in S/m. Using this quantity, the local temperature increase due to an applies  $SAR$  distribution can be calculated using:

$$SAR = \frac{C \cdot \Delta T}{\Delta t} \quad (3.2)$$

In which  $C$  is the specific heat capacity in  $\text{J}/(\text{kg } ^\circ\text{C})$ , and  $\Delta T/\Delta t$  is the change in temperature divided by the change over time in  $^\circ\text{C}/\text{s}$ .

In order to verify the simulations, the parameters of interest are the antenna's impedance, as well as its sensitivity to a change in temperature, input power target medium (see 3.1). The material properties of the setup, such as density and the dielectric properties, have also been measured.

#### 3.1 Construction of a fat and muscle equivalent phantom

A head and neck tissue mimicking phantom was created to mimic clinical conditions. This phantom consists of materials which electromagnetically, thermally and MRI technically represent human tissue. The phantom that is used in the experiments is an approximation of the human neck, and consists of two layers. The inner layer consists of a muscle equivalent material, while the outer layer represents a layer of human fat<sup>3</sup>. The dimensions of the phantom are shown in figure 3.1 and 3.2. The ingredients used to make the material as well as the steps followed in the construction of the phantom itself can be found in Appendix I.

The phantom needs to represent the human tissue in its dielectric properties, which consist of the permittivity ( $\hat{\epsilon}_r$ ), and the effective conductivity ( $\sigma_{eff}$ ). Both these properties have been measured and compared to earlier studies<sup>3</sup> after the phantom was finished. This is done by to measuring the properties of a sample of the material using a dielectric measurement kit in combination with a vector network analyser (VNA, see Appendix II for details), over a frequency range of 300-550 MHz. This way we also see to what extent its properties are frequency dependent.

To compensate for the effect of the sample's finite volumes, two measurements have been done. For one measurement the sample is mounted on top of a metal plate which reflects the signals that make it through the sample. The second measurement is performed with an absorber under the sample, to absorb all the signals that pass the sample. If the values of these two measurements are close to each other, the sample volume was large enough.

The VNA measures the complex relative permittivity of the material ( $\hat{\epsilon}_r$ ), in such a way that:

$$\hat{\epsilon}_r = \epsilon_r' - j\epsilon_r'' \quad (3.3)$$

where  $\epsilon_r'$  is the relative permittivity of the material, and  $\epsilon_r''$  is the complex part. Losses due to electric and dielectric heating are represented by the effective conductivity, which is given as:

$$\sigma_{eff} = \epsilon_r'' \epsilon_0 \cdot \omega \quad (3.4)$$

where  $\epsilon_0$  is the permittivity in free space and  $\omega$  is the angular frequency of the field.

While doing a measurement with de-mineralized water, it is determined that it takes 5 minutes for the results to converge to 0,2% of its final value. All the measurements, including the calibration, have therefore been done in five minutes. See also Appendix IV; "Time dependency of the dielectric measurement kit and the VNA".

Before starting the dielectric measurements of the muscle and fat mimicking materials, the dielectric measurement kit has been calibrated using a copper strip and ethanol. This way, a control measurement can be done using demi-water. This measurement can be compared to its literature value of  $\hat{\epsilon}_r=78$ , and  $\sigma_{eff}=0.04\text{S/m}^7$ .

In order to measure the dielectric properties of the muscle mimicking material, the probe of the dielectric measurement kit (see Appendix II) has to be pushed into the sample, and therefore may change the sample's properties. To ensure that this pressure doesn't influence the measurements, a set of measurements with varying pressures has been done. During those 7 measurements, the probe was pushed further into the sample, which resulted in a small layer of liquids showing on top of the sample. For the measurement of the fat sample, this effect was not seen.

Because of the relation of SAR to the density of the material, this has also been measured. The density however does not need to equal the density of the human tissue it represents, since this does not affect the radiation of the antenna. The material properties have also been measured for the phantom's plastic components, such as its outer shell.

Since the temperature of the phantom increases due to the radiation of the antennae, its material properties change. To measure if this affects the antenna's impedance, measurements with, and without phantom were compared.

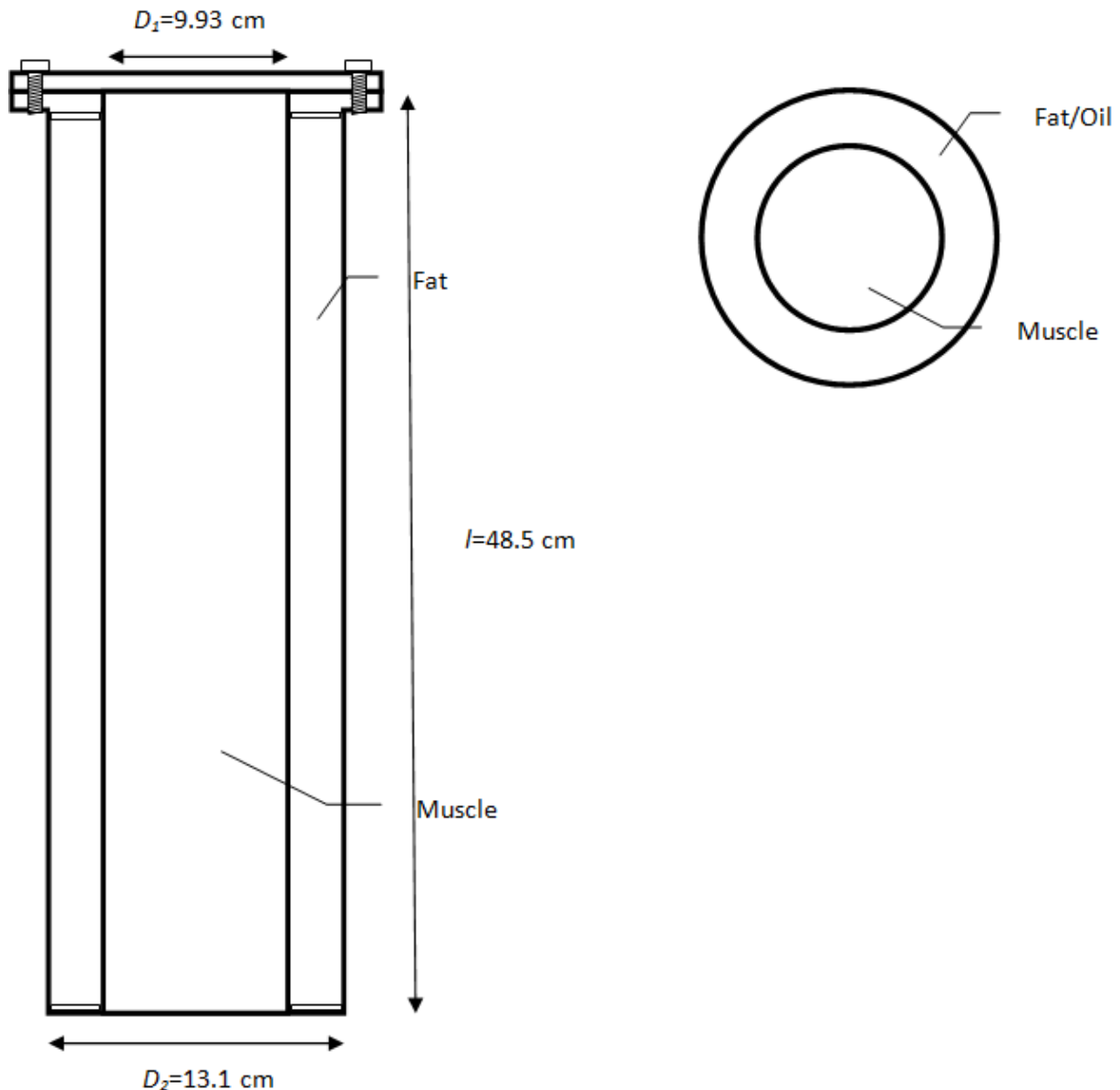


Figure 3.1 and 3.2; the front and top view of the neck representing phantom for the MRIlabcollar respectively.

### 3.2 Antenna base impedance

Although SEMCAD is great for simulating EM-waves, it is inaccurate in predicting the impedance of the antennae, while only knowing their dimensions and material properties. Because of this the impedance was found by measuring the antenna's  $RL$  values and using equation 2.2. The  $RL$  was measured using the VNA. Prior to this measurement, the phantom has been mounted into the MRIlabcollar. The measurements were performed at  $27 \pm 2^\circ\text{C}$ .

### 3.3 Sensitivity of the antenna impedance

We want to know to what extent the impedance of the antennae is sensitive to environmental variables. The quantities of interest are the temperature, the input power of the antennae and the dielectric properties of the used phantom, because of their variability in the setup.

### 3.3.1 Sensitivity to temperature and phantom material changes

As was shown in chapter 2.1, the impedance of the antennae depends on the properties of the radiation medium. As dielectric properties of water change with temperature<sup>7,8</sup>, so does the impedance of the antenna. To measure the sensitivity to the temperature of the antennae, two measurements have been done. First, the MRT collar was filled with 60 °C water, and slowly cooled down to 30 °C.  $S_{11}$  measurements for all antennae were performed after each 5 °C temperature drop. Prior to those  $S_{11}$  measurements, the water was stirred resulting in a homogeneous temperature distribution across the system. The second measurement was performed using an automated water circulator with an adjustable temperature setting. The water was first cooled down to 15 °C and slowly warmed up to 35 °C. At every increase of 5 °C, the  $RL$  of all the antennae has been measured. The two different measurements were necessary since the water circulator its inability to warm the water above 45 °C.

In order to measure the phantom's effect on the antenna's impedance,  $S_{11}$  measurements were performed with and without the phantom at the centre of the MRIlabcollar, and compared.

### 3.3.2 Sensitivity to input power

Some of the power offered to the antennae is transformed into heat. This influences the antenna's impedance, so we measured the impedance change over time for different powers using the setup described in Appendix III. Prior to each measurement, the starting temperature of the circulatory water was set to 30 °C. While the power was fed to the antennae, the circulator was turned off so that the water can increase its temperature.

Two different measurements have been done. The first one is done by feeding 120W of power to three different antennae and measuring their  $RL$  every five minutes during 15 minutes, to see how long it takes for the antenna to reach its final temperature. During the second measurement we started at 20W, and increased the power to 140 with steps of 20 watts. After increasing the power, we waited for 20 minutes after which we measured the temperature at the antenna's connector using an electric thermometer and recorded the  $RL$ .

## 3.4 Coupling measurements

In order to measure the  $FTC$ , two antennae were connected to the VNA for  $S_{21}$  measurements. During these measurements, the other ten antennae were terminated, so that the energy they absorb will not be reradiated. Measurements have been done for all antennas, so that a twelve by twelve matrix of  $FTC$  values was formed. During the experiment, the phantom was mounted into the MRIlabcollar.

## 4. Results and discussion

In this chapter, the results of the measurements are shown and discussed

### 4.1 Dielectric properties of the phantom

Figure 4.1 and table 4.1 show that the variance in pressure hardly affects the results. All shown values correspond with a frequency of 434 MHz. During the first measurement, the probe was not in good contact with the sample, resulting in false values. The other measurements show a relative permittivity of  $52 \pm 2$ , and an effective conductivity of  $0.84 \pm 0.04$  S/m. These uncertainties lie within the 5% range of the VNA its uncertainty, as shown in Appendix III. These obtained values correspond with earlier found values of  $\epsilon_r' = 55.30 \pm 1.74$  and  $\sigma_{eff} = 0.759 \pm 0.032^3$

Since the fat mimicking material never solidifies, variety in pressure is not a problem. This can be seen in table 4.2, where the measured values for 434 MHz for two different samples of the same phantom are shown, while applying an increasing pressure. We find a small change in the relative permittivity of the two samples, showing that there is some variation within the material, which was not seen for the muscle samples. This might be a result of air bubbles trapped in the sample. These air bubbles are also seen in the phantom itself, since the removal of them is challenging. The values of the fat sample are  $\epsilon_r' = 4.5 \pm 0.2$  and  $\sigma_{eff} = 28.6 \pm 0.1$  mS/m. These acquired are lower than earlier found values of  $\epsilon_r' = 6.78 \pm 0.73$  and  $\sigma_{eff} = 34 \pm 6^3$ . This might be a result of the earlier mentioned air bubbles.

The dielectric properties of the plastic used in the phantom have also been measured, using the lids that are used to close off the phantom. These lids have a radius of 85.0 mm and a thickness of 9.8 mm. The first two measurements were performed by placing a lid on a metal surface, and compare the results with the same lid on top of a layer of air. As can be seen in table 4.3, the results between the first two measurements show a change of over 5%. Since this might indicate that the dimensions of the sample are too small, two lids were screwed together, and the dielectric properties were measured at both sides of the lids. As can be seen in table 4.3, the relative permittivity still showed a change in its value of over 5%. This effect might be a result of the surface of the plastic being rough, allowing air between the probe and the sample. Another difference between the plastic, and the muscle or fat sample, is that the plastic does not enclose the probe when it is pushed on the sample. Taking these uncertainties in mind, the relative permittivity is  $2.5 \pm 0.5$  and the effective conductivity  $0.008 \pm 0.002$ .

The density of the phantom materials and the plastic has also been measured. For the plastic, and the muscle and fat sample a density of 1.19, 0.94 and 1.01 g/cm<sup>3</sup> was measured respectively. The literature density for muscle and fat are respectively 1.06<sup>4</sup> and 0.92<sup>5</sup> g/cm<sup>3</sup>.

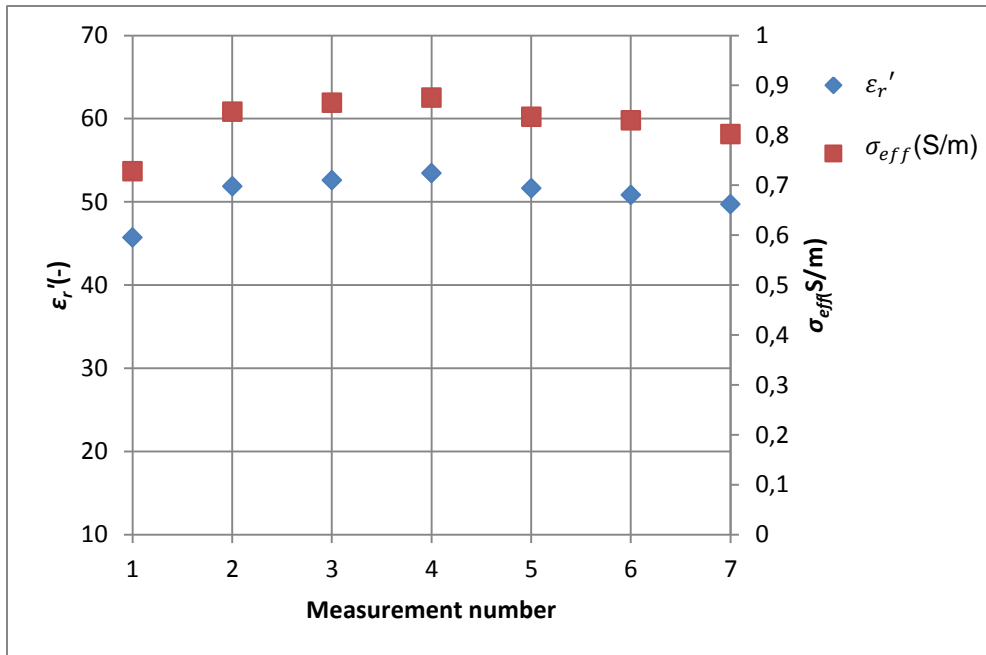


Figure 4.1; the measurement of  $\epsilon_r'$  and  $\sigma$  for the muscle mimicking material. The probe was pushed further into the sample every measurement. All measurement points correspond to the values at 434 MHz.

Table 4.1; the measurement as shown in figure 4.1. For each measurement, the probe was pushed further into the sample.

#	$\epsilon_r'$	$\sigma_{eff}$ (S/m)
1	45,7	0,73
2	51,9	0,85
3	52,6	0,87
4	53,5	0,88
5	51,6	0,84
6	50,8	0,83
7	49,7	0,80

Table 4.2; the measurement of  $\hat{\epsilon}_r$  and  $\sigma$  for the fat mimicking material. Two different samples were measured, both from the same phantom. The first 4 measurements are done with the first sample, while the second 4 measurements are done with the second sample. Both samples have been measured while applying a increasing pressure. All measurement points correspond to the values at 434 MHz. The ninth measurement is done with demi-water as a control.

#	$\epsilon_r'$	$\sigma_{eff}$ (mS/m)
1. sample 1	4.7	28.6
2. sample 1	4.7	28.6
3. sample 1	4.7	28.6
4. sample 1	4.7	28.6
5. sample 2	4.3	28.6
6. sample 2	4.4	28.6
7. sample 2	4.4	28.6
8. sample 2	4.4	28.5
9. demi-water	70.0	84.8

Table 4.3; 5 different measurements for the dielectric properties of the plastic used for the phantom. The first measurement is done by placing the lid air, and the second on metal. The third and fourth measurements are done by screwing both lids together, and measuring from both sides. All measurement points correspond to the values at 434 MHz. The fifth measurement is done with demi-water as a control.

#	$\epsilon_r'$	$\sigma(\text{S/m})$
1. one lid on air	2.57	0.0050
2. one lid on metal	2.27	0.0072
3. two lids	2.19	0.0083
4. two lids	2.68	0.0088
5. demi-water	71.3	0.092

## 4.2 Antenna base impedance

There are a total of 12 antennae mounted in the MRlabcollar. These antennae are divided into two rings. Each antenna has a number referring to its position. The first number refers to the row it is in (1 or 2), and the second number gives the number of the antenna in the row (1 to 6). The antennae are numbered 1\_1 to 2\_6, see figure 1.1. Table 4.4 shows the  $RL$  per antenna and the corresponding impedance. The data for the other antennae is shown in Appendix IV; “ $S_{11}$  measurements”. All measurements were performed at a temperature of  $27 \pm 2$  °C

Table 4.4; the measured  $RL$  values for all 12 antennae, and the corresponding impedance. All measurement points correspond to the values at 434 MHz.

Antenna #	$ S_{11} ^2$ (dB)	$Z$ ( $\Omega$ )
1_1	-19.91	57.38 + 8.00j
1_2	-10.21	81.36 - 27.04j
1_3	-15.71	54.06 - 16.80j
1_4	-15.58	56.33 - 16.75j
1_5	-20.52	54.29 - 8.87j
1_6	-16.50	54.89 - 15.08j
2_1	-13.82	69.32 - 15.06j
2_2	-13.16	71.49 - 16.27j
2_3	-17.89	62.82 - 6.58j
2_4	-19.25	60.62 - 5.75j
2_5	-18.54	63.38 - 0.95j
2_6	-17.64	57.58 - 12.02j

Most values are close to the intended 50  $\Omega$ , with an additional phase shift. Antenna 1\_2 is the furthest away with its 81.36  $\Omega$ . Additional measurements done with antenna 1\_2 show that the measured return loss changes if the coax cable, which connects the antenna to the VNA, is moved. This effect is not apparent for the other antennae, indicating that antenna 1\_2 is not properly connected to the MRlabcollar. The  $S_{11}$  results as shown figure 4.2 and 4.3, show that this antenna is off for the other frequencies as well. Appendix IV; “ $S_{11}$  measurements” shows the  $RL$  for the other antennae in individual graphs. Some additional measurements were done to determine the error in  $RL$  for antenna 1\_2. The results are shown in Appendix IV; “antenna 1\_2”.

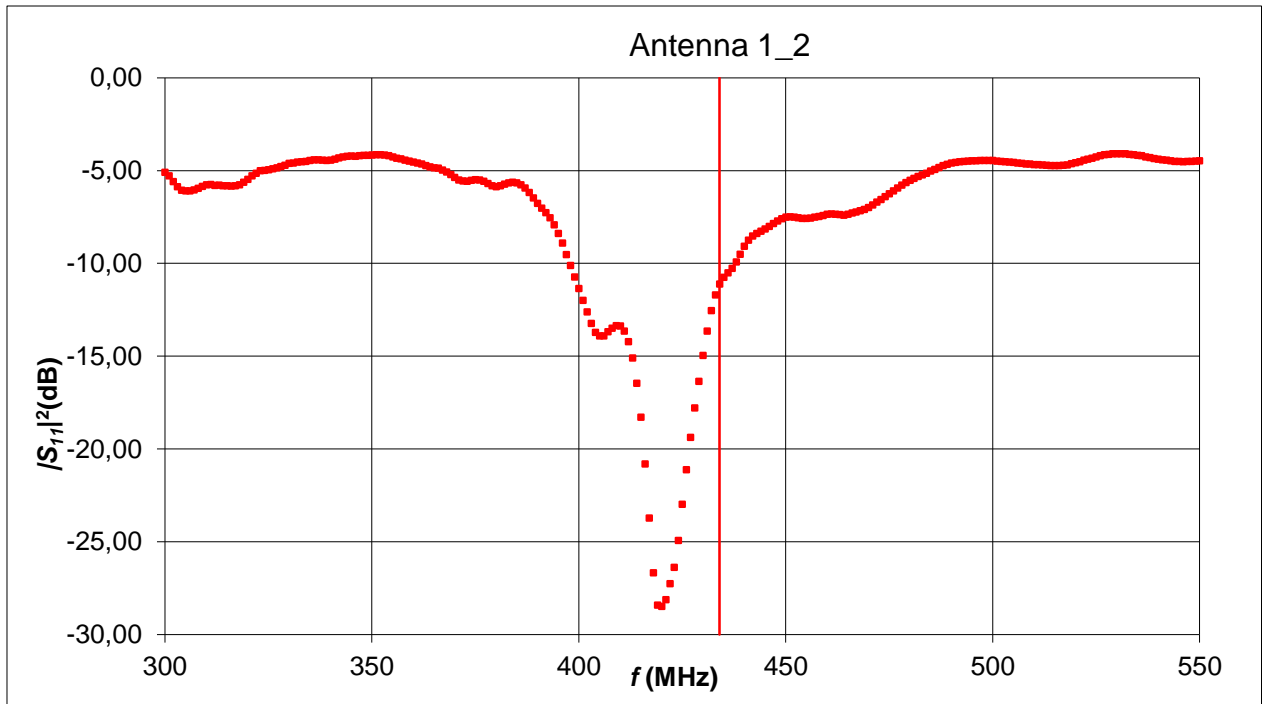


Figure 4.2; the RL of antenna 1\_2.

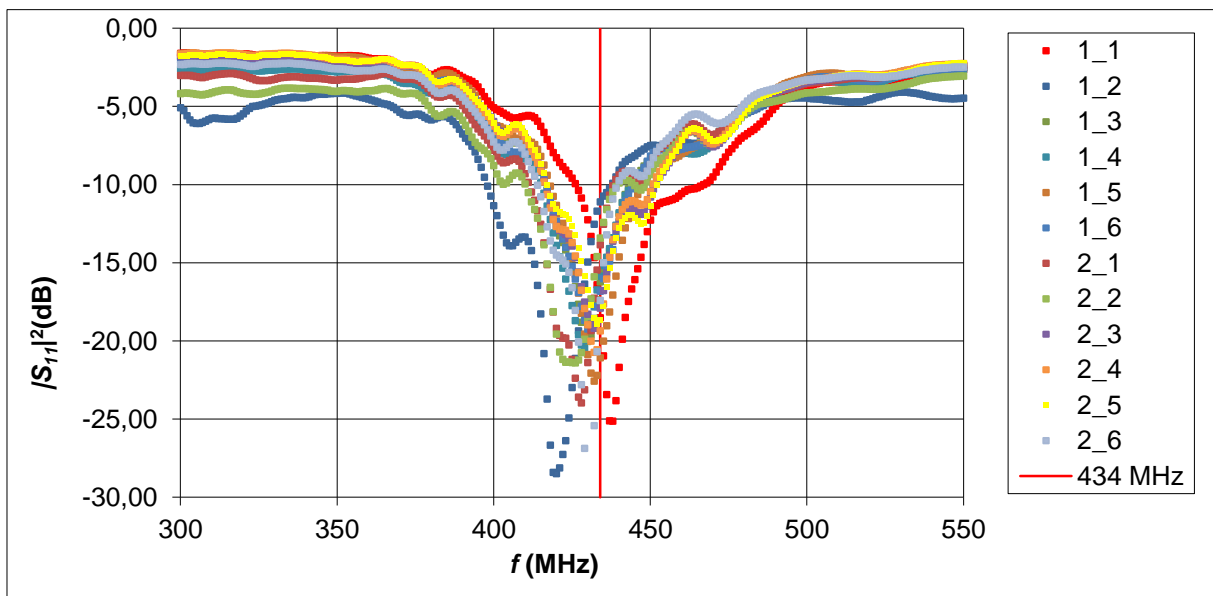


Figure 4.3; The RL values of antenna 1\_2, as well as its values in comparison with the other antennae.

### 4.3 Sensitivity of the antenna impedance

This sub chapter is divided into three parts, respectively showing the results of the phantom sensitivity, temperature sensitivity and the power sensitivity.

#### 4.3.1 Phantom sensitivity

The properties of the antenna seem to be unrelated to the presence of the phantom. As is seen in the  $S_{11}$  results as shown in figure 4.4, there is hardly any difference between the measurements with, or without the phantom. This shows us that the phantom lies in the far field of the antenna, and influence is negligible. Figure 4.5 shows the RL of antenna 1\_1 with and without a phantom, for comparison. Note that in figure 4.4, the effect of the phantom shows most for antenna 1\_2. This antenna however does not supply valid measurements, since moving the coax cable results in a change of measurement, as explained in 4.2 and shown in Appendix IV, "antenna 1\_2".

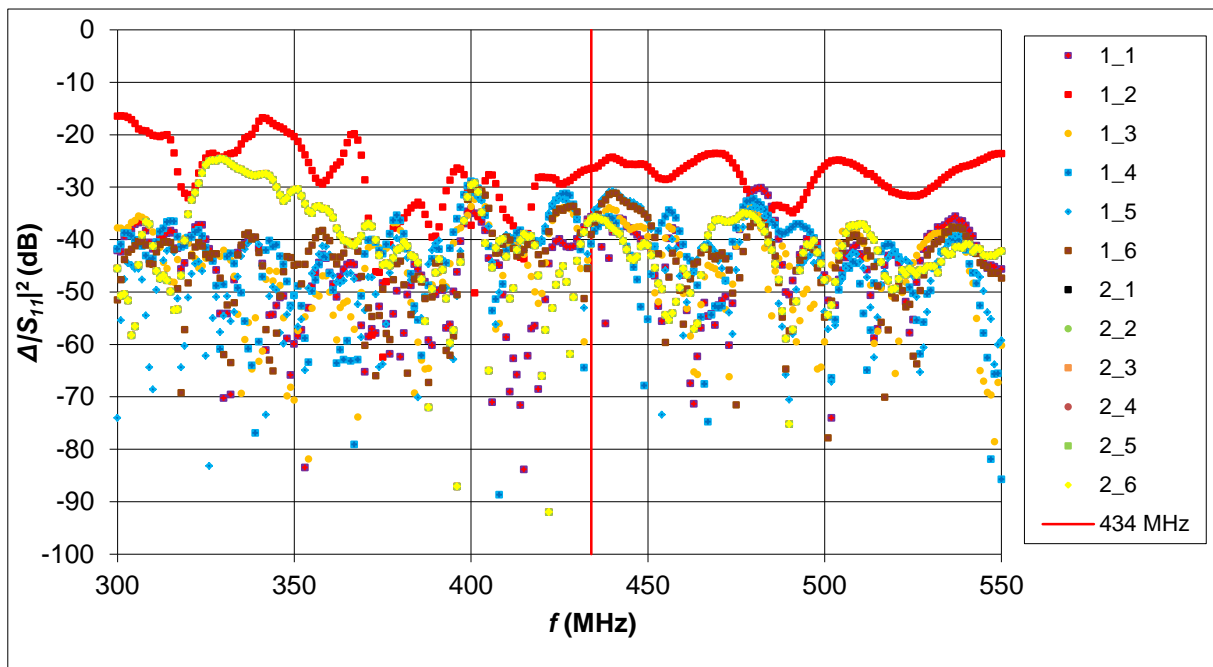


Figure 4.4; the effect of the phantom on the RL of the antennae. The vertical axis represents the difference between the RL value with, and without the phantom, in a logarithmic scale.

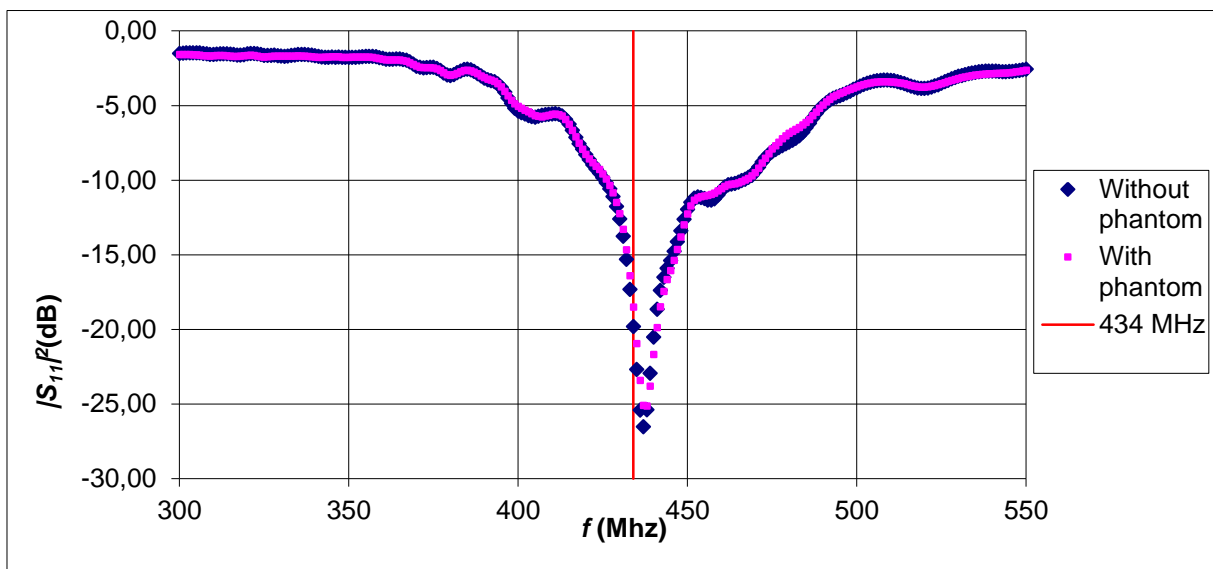


Figure 4.5; the  $S_{11}$  measurements with and without the phantom for antenna 1\_1. The other antennae show similar results.

#### 4.3.2 Temperature sensitivity

In figure 4.6 is shown that the RL value is affected by the temperature of the medium, in which the antennae are submerged. As is seen in table 4.5, the  $f_{res}$  decreases with the rate of about 0.8 MHz/°C, or -2 MHz/ $\epsilon_r$ . These effects have been found earlier<sup>6,7</sup>. The optimum operating temperature for the antenna is 30 to 35°C. This is in agreement with the values shown in table 4.6, where the averaged RL is shown for the same temperature range.

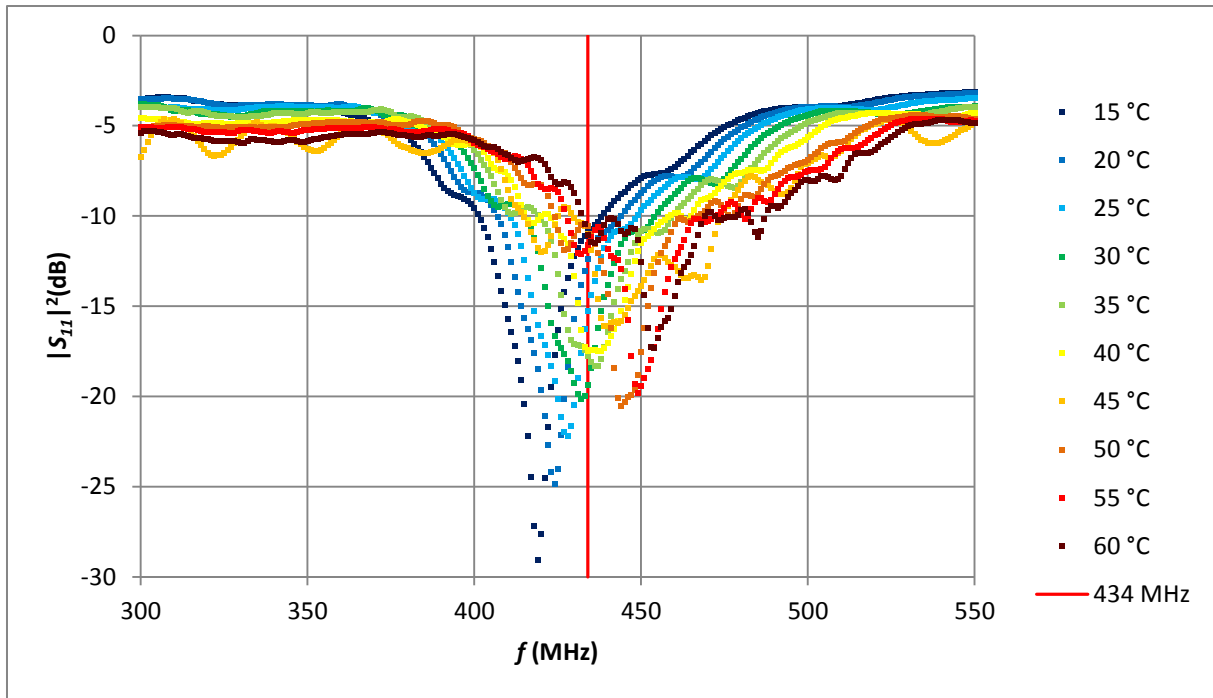


Figure 4.6; the effects of temperature on the  $S_{11}$  measurements of the antennae. This graph shows the RL, averaged over all twelve antennae. All seven temperatures have been plotted for comparison.

Table 4.5; the  $f_{res}$  for a temperature range from 15 to 60 degrees, averaged over all twelve antennae, measured by two separate measurements.

$T$ (°C)	15	20	25	30	35	40	45	50	55	60
$\hat{\epsilon}_r$ (-)	82	80	78	76	74	72	70	68	66	64
$f_{res1}$ (MHz)	419	424	428	432	436					
$f_{res2}$ (MHz)				429	434	436	439	444	449	454

Table 4.6; the RL at 434 MHz for a temperature range from 15 to 60 degrees, averaged over all twelve antennae, measured by two separate measurements.

$T$ (°C)	15	20	25	30	35	40	45	50	55	60
$\hat{\epsilon}_r$ (-)	82	80	78	76	74	72	70	68	66	64
$ S_{11} ^2_1$ (dB)	-10.9	-12.4	-15.2	-19.4	-17.7					
$ S_{11} ^2_2$ (dB)				-16.9	-19.4	-17.5	-11.0	-10.6	-11.6	-11.0

### 4.3.3 Power sensitivity

For the first measurement, 120W was fed to three different antennae in three separate measurements. As is seen in figure 4.7, the RL for the antennae increases when the power is fed. This is in agreement with the temperature sensitivity measurement, where we found that at 30 °C, the  $f_{res}$  lies closest to 434 MHz. It is found that within five minutes, the temperature has reached its final value.

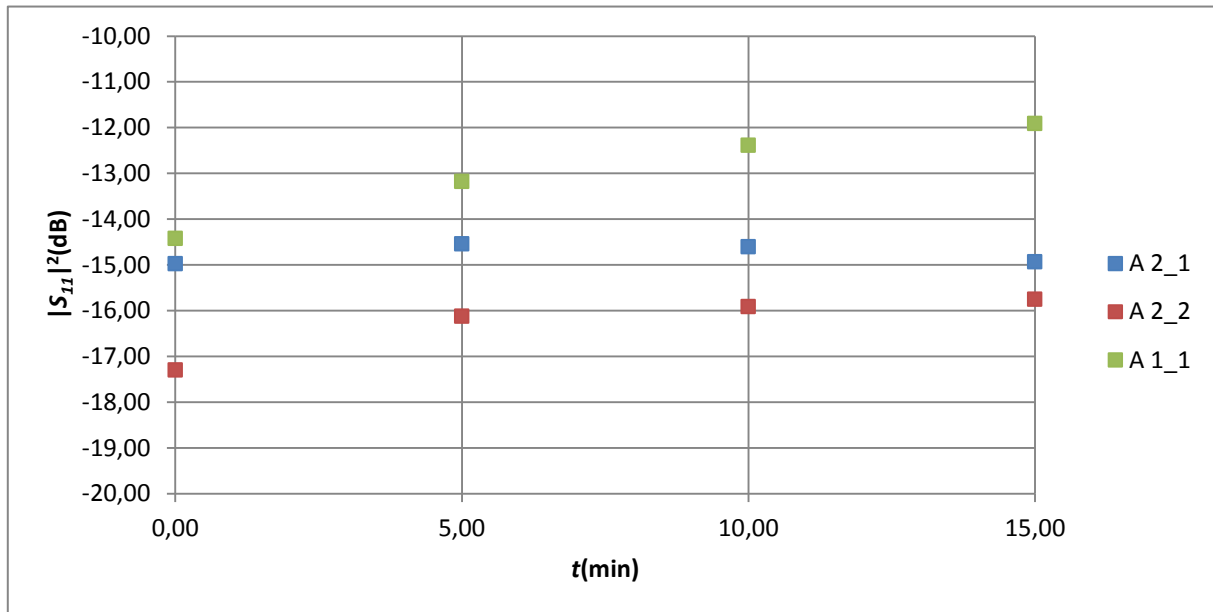


Figure 4.7; 120W was fed to three antennae, while every five minutes the  $RL$  was measured.

Following this, the power was increased in steps of  $\sim 25$  W for antenna 1\_1. After each step we waited 20 minutes prior to the measurements, to make sure that the temperature has stabilised. In figure 4.8, the temperature and  $RL$  are plotted against the input power. Note that at  $P=23$  W, two measurements were done. The first at  $t=0$  min, and the second at  $t=20$  min. Both the temperature and the  $RL$  did not change, resulting in the measurement points overlapping. The relation between the  $RL$  in dB and the input power is linear for the power range of 20 to 140 W, and increases from -16, to -8 dB. The relation between the input power to the temperature is linear for this range as well, increasing from 30 to 78 °C.

Interestingly, this linear relation between the temperature and the  $RL$  of the antenna has also been found for the temperature sensitivity of the antenna's  $RL$ , but with a different factor. Figure 4.9 shows the  $RL$  for a temperature range of 15 to 60 °C for antenna 1\_1, as found in the temperature sensitivity study. For 30 to 60 degrees, the second measurement also shows a linear relation ( $R=0.90$ ), with a different factor. For this temperature increase, the  $RL$  increases from -12 to -5dB. This different factor might be the result of the temperature distribution of the measurements. For the temperature sensitivity study, the temperature was homogeneously distributed, while for the power measurement, the water was heated by the antenna. As seen in figure 4.10, the warm water flows to the top of the MRlabcollar. Since antenna 1\_1 is mounted on top of the MRlabcollar, the temperature of the lowest part of the antenna may be different from the temperature at the top.

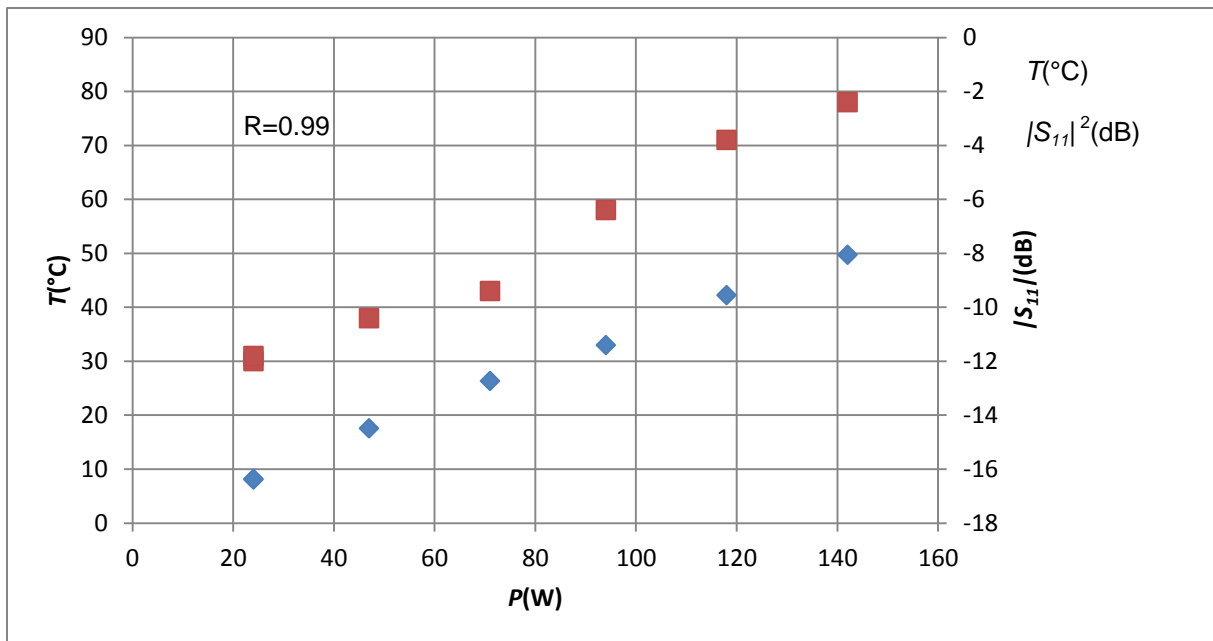


Figure 4.8; the change of temperature and RL caused by the change in input power. Within the power range of 20-140W, there is a linear relation between the two.

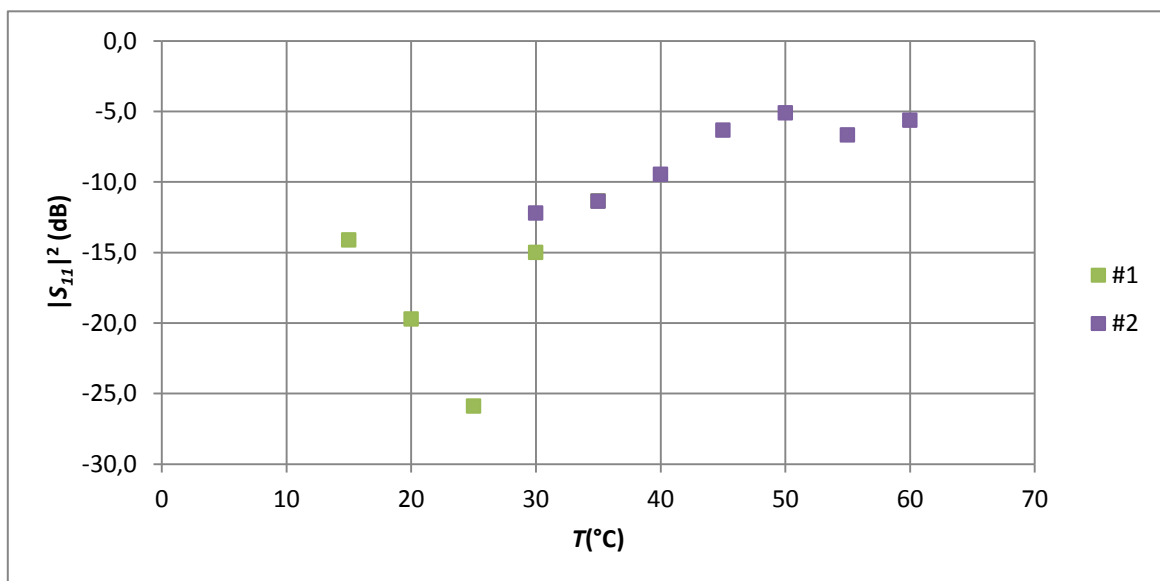


Figure 4.9; the RL for antenna 1\_1 at different temperatures, obtained by two different measurements as described in 3.3.

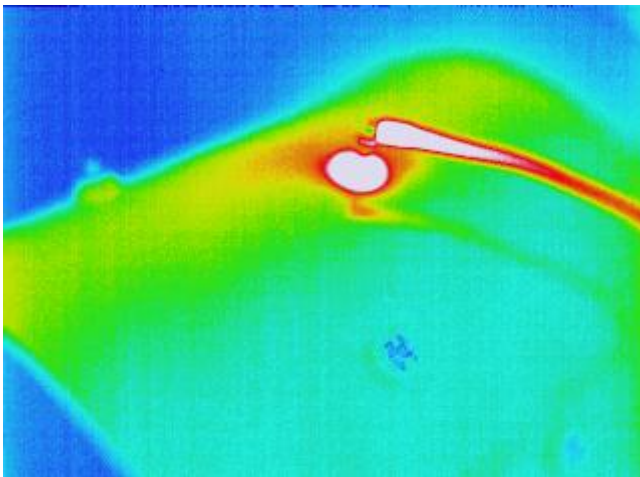


Figure 4.10; the temperature distribution while having power on the antenna. The absolute temperatures cannot be measured, though it is clear that the top of the MRlabcollar is warmer than the bottom. This picture was taken using a infra-red camera. The blue spot below the powered antenna is another (unpowered) antenna. The red line coming from the antenna is the cable. A reflection of this cable can also be seen.

#### 4.4 Coupling measurements

The  $FTC$  has been measured for all antennae. Figure 4.11 shows the coupling values for antenna 1\_1 for the frequency range of 300 to 550 MHz. The  $FTC$  between two individual antennae lies below  $-15.5\text{dB}$  for all measurements at 434 MHz, and is  $-20.3$  on average. Compared to the  $FTC$  values of the original H&N applicator, which measured a maximal  $FTC$  of  $-22$ , and an average  $FTC$  of  $-27\text{dB}$ <sup>7</sup>, the values have increased. Figure 4.12 shows the  $FTC$  for antenna 1\_1 for 434 MHz, while displaying a schematic of the MRlabcollar setup. This schematic shows that the amount of coupled power changes with the angle between the two antennae. This might be explained by the radiation pattern of patch antennae. As shown in figure 4.13, (patch) antennae can radiate in patterns where the intensity of the bundle varies up and down when changing the angle. Both figures 4.11 and 4.12 can be found for all antennae in Appendix IV; “ $S_{21}$  measurements, Graphs” and “values at 434 MHz” respectively.

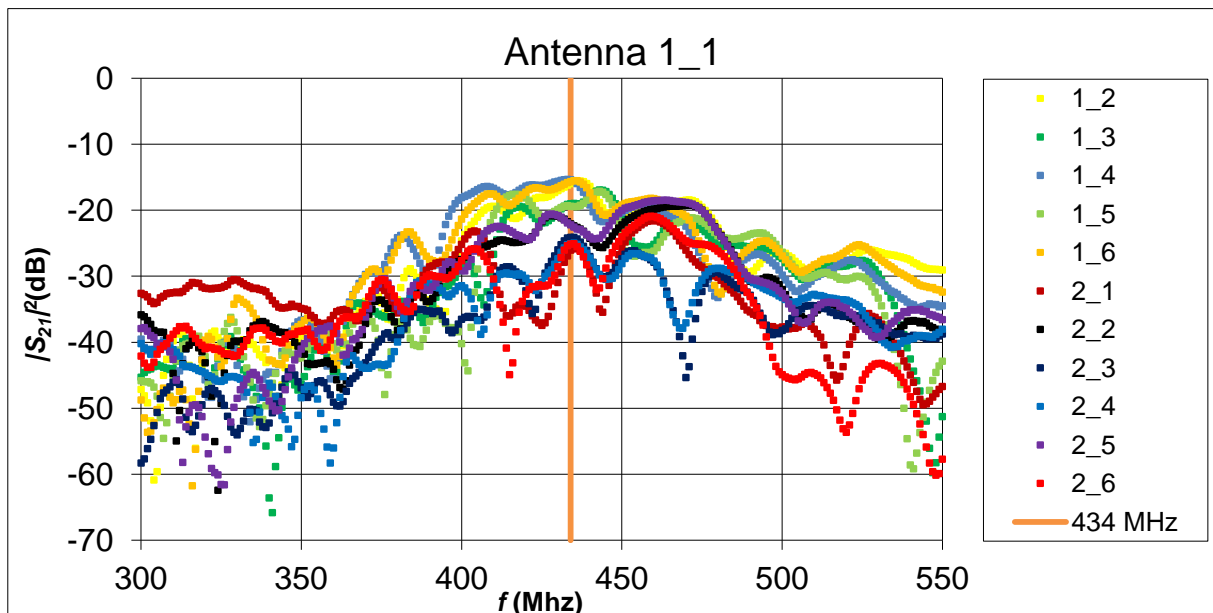


Figure 4.11; the coupling values for antenna 1\_1, from all other antennae. At 434 MHz, the maximum  $FTC$  value is  $-16.3\text{dB}$ , and comes from antenna 1\_6.

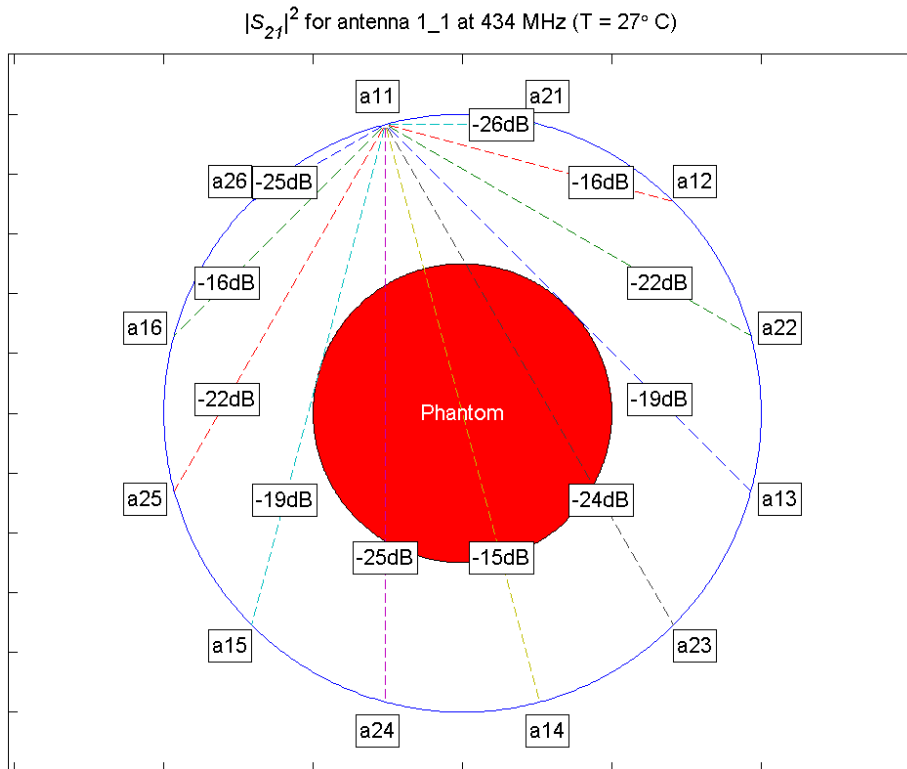


Figure 4.12; the coupling measurements for antenna 1\_1 at 434 MHz.

Table 4.7 shows the worst case coupling (WCC) per antenna. This coupling is found by adding all the coupling values for one antenna together. The highest value at 434 MHz is calculated at -7.1dB. Note that this value is measured for antenna 1\_2 and therefore might not be valid, as shown in Appendix IV; "Antenna 1\_2".

Table 4.7; the worst case coupling (WCC) per antenna.

Antenna	1_1	1_2	1_3	1_4	1_5	1_6	2_1	2_2	2_3	2_4	2_5	2_6
WCC(dB)	-8.5	-7.1	-8.9	-9.0	-9.8	-9.4	-8.0	-7.9	-8.7	-8.7	-8.7	-8.7

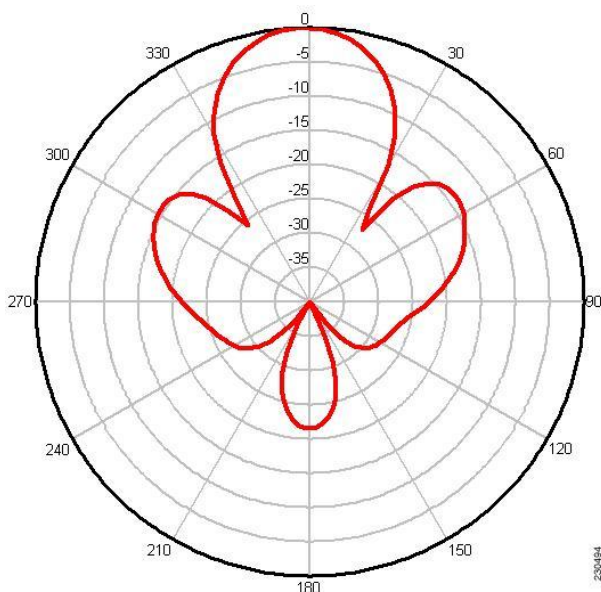


Figure 4.13; a possible radiation pattern for a patch antenna<sup>12</sup>

## Conclusion

A human neck mimicking phantom has been fabricated. It consisted of an outer layer of fat mimicking material, and an inner cylinder of muscle mimicking material, separated by a plastic layer. The dielectric properties have been measured and successfully compared to literature values. Furthermore, the density of all the materials of the phantom, including the plastic, has been measured.

The coupling between two antennae at 434 MHz lies around -16dB. This results in a total coupling, or worst case coupling of -8dB to -9dB.

The antenna's impedance, as well as its sensitivity to the phantom, temperature and input power has been measured using their return loss. The phantom had no significant effect on the antenna's  $RL$ , while the temperature of the medium surrounding the antenna did. For a resonance frequency of 434 MHz, a temperature between 30 to 35 °C proved optimal. For higher or lower temperatures, the  $RL$  at 434 MHz increased. For an input power between 25 and 140 watt, the  $RL$  increased linearly to the increasing input power from -16 to -8 dB.

Antenna 1\_2 shows changing  $RL$  values when the cable it is attached to is moved. This effect is absent for the other antennae, indicating that this antenna might be loosely connected.

## References

1. Cancer is a Preventable Disease that Requires Major Lifestyle Changes, Preetha Anand, Ajaikumur B. Kunnumakara, Chitra Sundaram, Kuzhuvellil B. Harikumar, Sheeja T. Tharakan, Oiki S. Lai, Bukyung Sung and Bharat B. Aggarwal, 2008
2. "Re-setting the biological rationale for thermal therapy" *Int J Hyperthermia*, 21:779-790, MW Dewhirst, Z Vujaskovic, E Jones and D Thrall, 2005
3. "A heterogeneous human tissue mimicking phantom for RF heating and MRI thermal monitoring verification", Yu Yuan, Cory Wyatt, Paolo Maccarini, Paul Stauffer, Oana Craciunescu, James MacFall, Mark Dewhirst and Shiva K Das, 2012
4. "Specific Force Deficit in Skeletal Muscles of Old Rats Is Partially Explained by the Existence of Denervated Muscle Fibers", *The Journals of Gerontology Series A: Biological Sciences and Medical Sciences* **56** (5): B191–B197, Urbancheka, M; Pickenb, E; Kaliainenc, L; Kuzon, 2001
5. "Association of adiponectin and resistin with adipose tissue compartments, insulin resistance and dyslipidaemia", *Diabetes, obesity & metabolism* **7** (4): 406–13. Farvid, MS; Ng, TW; Chan, DC; Barrett, PH; Watts, 2005
6. Farvid, MS; Ng, TW; Chan, DC; Barrett, PH; Watts, GF (2005). 6. Effects of Temperature Variations on Microstrip Antenna, Ravindra Kumar Yadav, Jugul Kishor, Ram Lal Yadava, 2012
7. "Development of a clinical head and neck hyperthermia applicator", PhD Thesis, Maarten Paulides, 2007
8. The complex dielectric constant of pure and sea water from microwave satellite observations, Thomas Meissner, Frank Wentz, 2004
9. Globocan 2008, IARC, 2013
10. "Antenna theory: Analysis and design", John Wiley & Sons, INC., New York, 2<sup>nd</sup> edition, CA Balanis, 1997
11. "Evolving technology for thermal therapy of cancer", *Int J Hyperthermia*, 21:731-744, PR Stauffer, 2005
12. <http://www.cisco.com/en/US/docs/wireless/antenna/installation/guide/ant5114P.html>, 2013

## Appendix I: Fabrication of a fat and muscle equivalent phantom

The phantom consists of a plastic object in which there are two compartments. The inner compartment is filled with muscle equivalent material, while the outer compartment is filled with a fat equivalent material. The dimensions of the phantom are shown in figure 2.1.

### Muscle equivalent material

The following table shows the ingredients that have been used for the muscle mimicking phantom.

Ingredients:	$m(g)$ :
Demi-water	3898.0
Salt (iodized)	21.3
Polyethylene (PEP)	278.5
Agar	116.4
TX-151	107.4
Formaldehyde (4%)	37.2
Gadolinium	0.2ml

In order to make the phantom, the water was heated up to 80 °C when the agar was added. This had to be mixed very good in order to become a homogeneous solution, though not too fast, to avoid air mixing with the water. After this process, at 72 °C, the PEP, tx-151 and salt were added. During the new period of mixing, the formaldehyde was added, as well as the gadolinium. After this the muscle phantom is poured into the inner cylinder of the phantom and closed up, to avoid dehydration.

### Fat equivalent material

The following table shows the ingredients that have been used for the fat mimicking phantom.

Ingredients:	$m(g)$ :
Demi-water	430.1
Oil	2464.1
Surfactant	278.5
Salt	0.6
Gelatine	80.0
Formaldehyde	18.9ml

First the water is heated up to 90 °C. After this the gelatine and salt were added. After this the oil was heated up to 60 °C and added in steps of increasing amounts, starting with 100 grams. Every time the oil was added, some surfactant was added as well, to improve the mixing of the oil and the water. During this process, the mixing is very important. If you stir too much, the gelatine starts to solidify. If you stir too little, the oil and the water will dissociate and leave an inhomogeneous phantom. The final step is the addition of the formaldehyde.

## Appendix II: VNA and dielectric measurement kit

A Vector network analyser is an instrument that is used to measure network parameters, such as S-parameters. It has two ports, out of which it can transmit and receive signals. It consists of a variable frequency source, which can connect to any of the two ports. For  $S_{11}$  measurements, port 1 is used for transmitting, as well as receiving signals. The output and input are compared by the device and the S value is displayed. For the  $S_{21}$  measurements, two ports are required, one input, and one output. The VNA used for the measurements is a ZNC3 Rhode& Swarts Vector Network Analyser. In the documentation, a 5% uncertainty has been stated.

In order to perform dielectric measurements, the VNA is coupled to a dielectric measurement kit. The main part of this is a probe, which consists of a transmitting, and a receiving part, see figure A.1. The VNA generates a range of frequencies which pass through the probe and the tissue sample. The VNA measures the return values and gives the dielectric properties of the sample. The dielectric measurement kit used for the measurements is a Schmid & Partner Engineering AG dielectric measurement kit.



Figure A.1; the probe used for the dielectric measurements.

### Appendix III: Power measurement setup

For the power measurements we used a medical amplifier which can produce up to 200 W at the frequency of 343.92 MHz. As is seen in figure A.2, a part of this is coupled to a wattmeter with a gain of -40 dB, while the rest of the power is transferred to another power coupler, which couples -42 dB to port one of the VNA. The remaining power is sent to the antenna, which reflects a part of it. -42 dB of this reflected power is measured by the VNA on port two, so that the  $RL$  can be calculated by dividing the input of port two by port one. The rest of the reflected power is absorbed by the amplifier, which has a heat sink built into it. The total power loss from the amplifier to the antenna has been measured at -0.2 dB. The starting temperature for the water surrounding the antennae is 30 °C. During the experiment the water was not circulated.

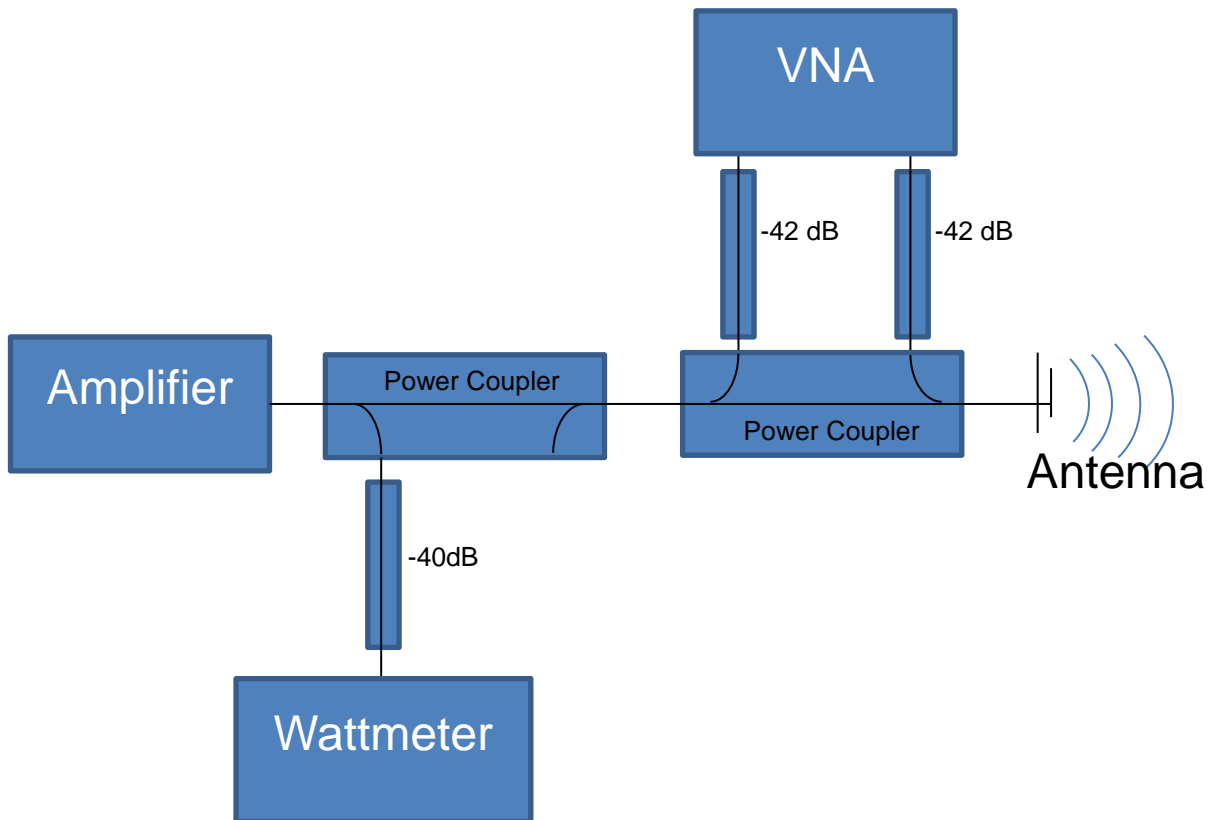
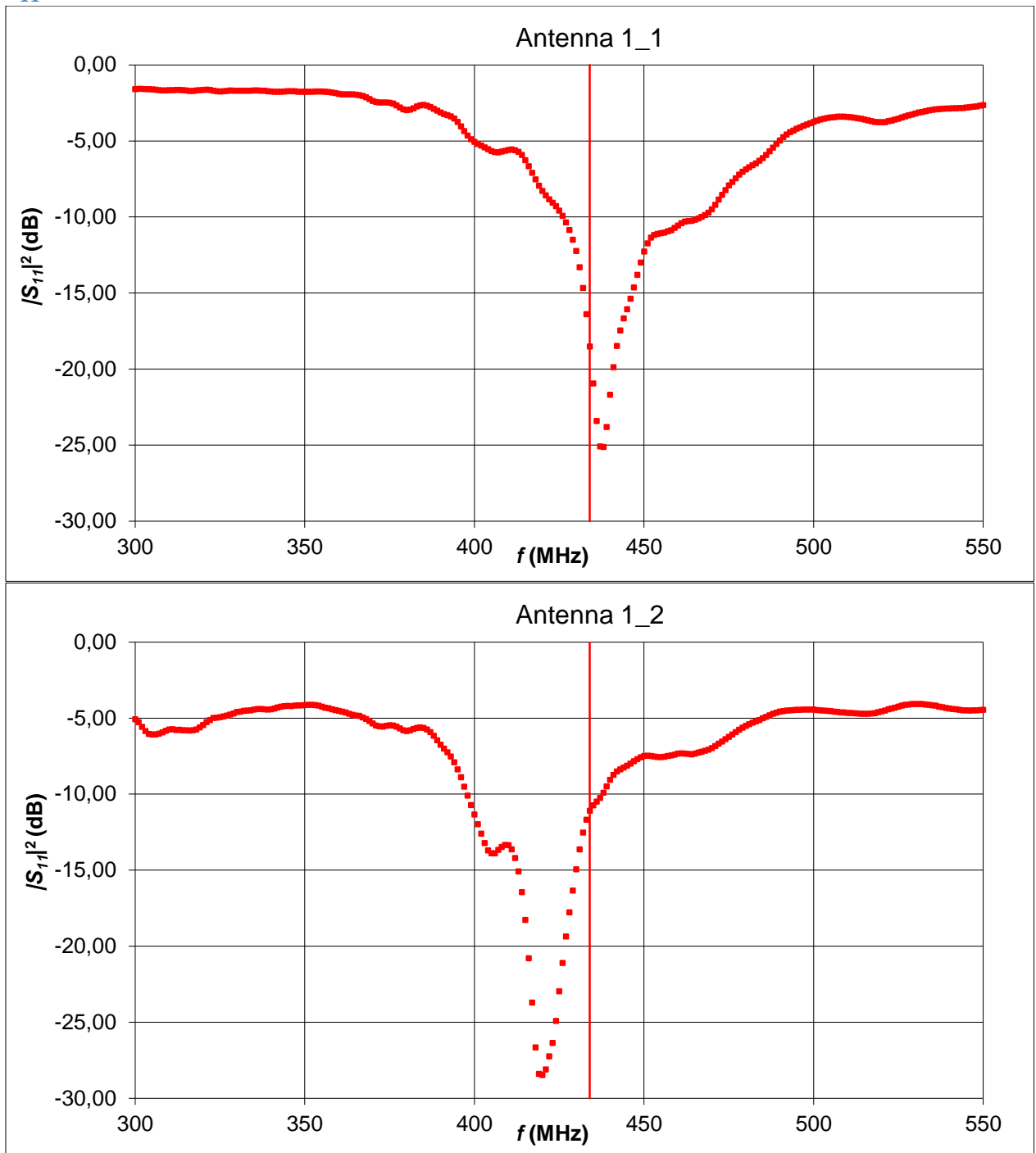
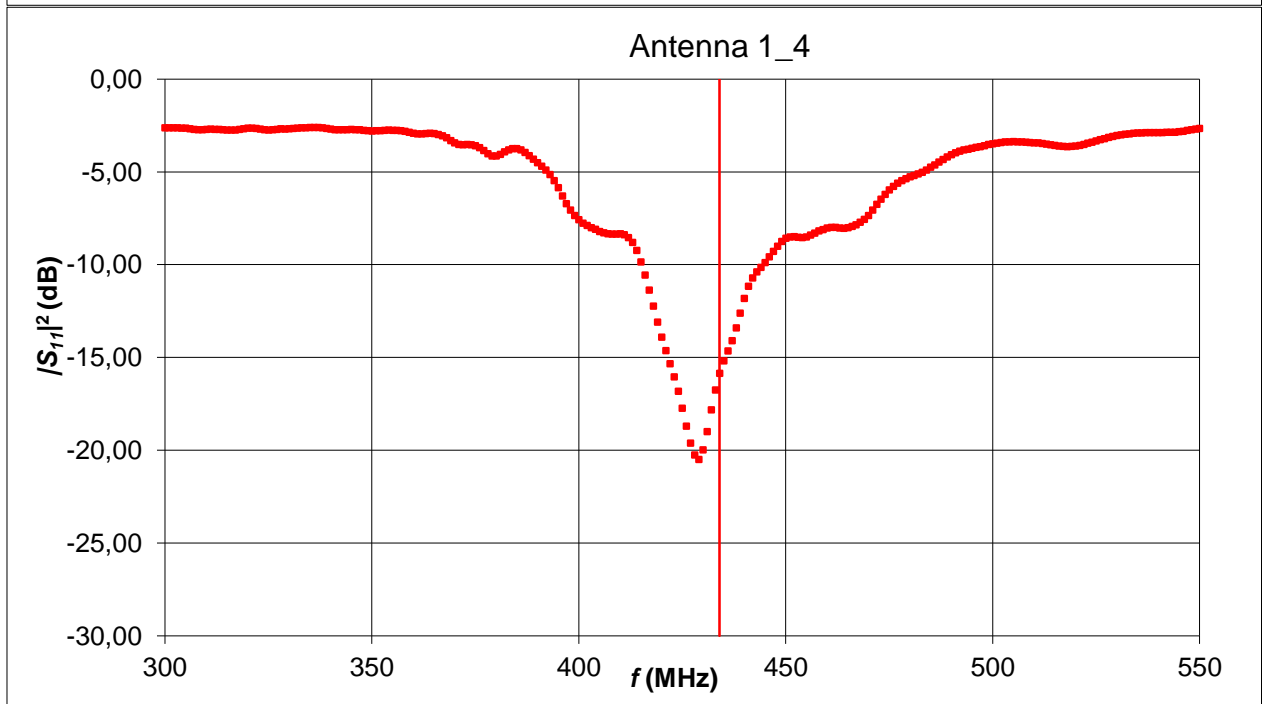
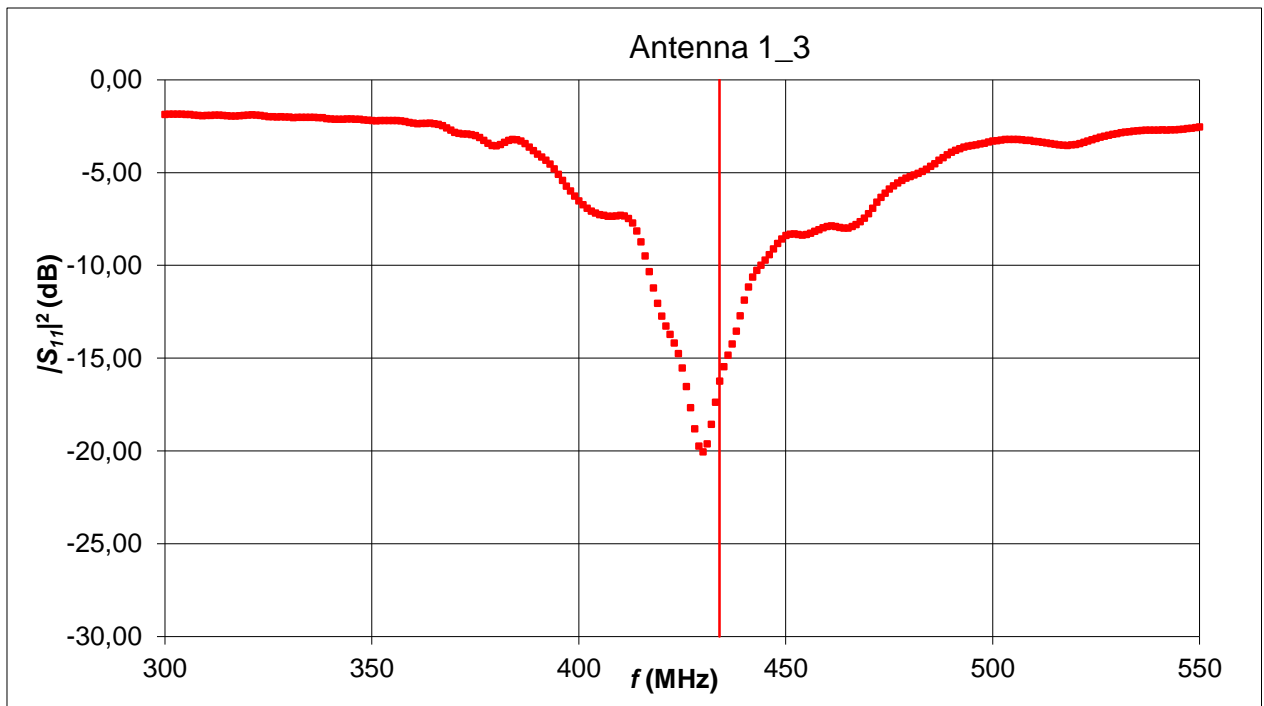


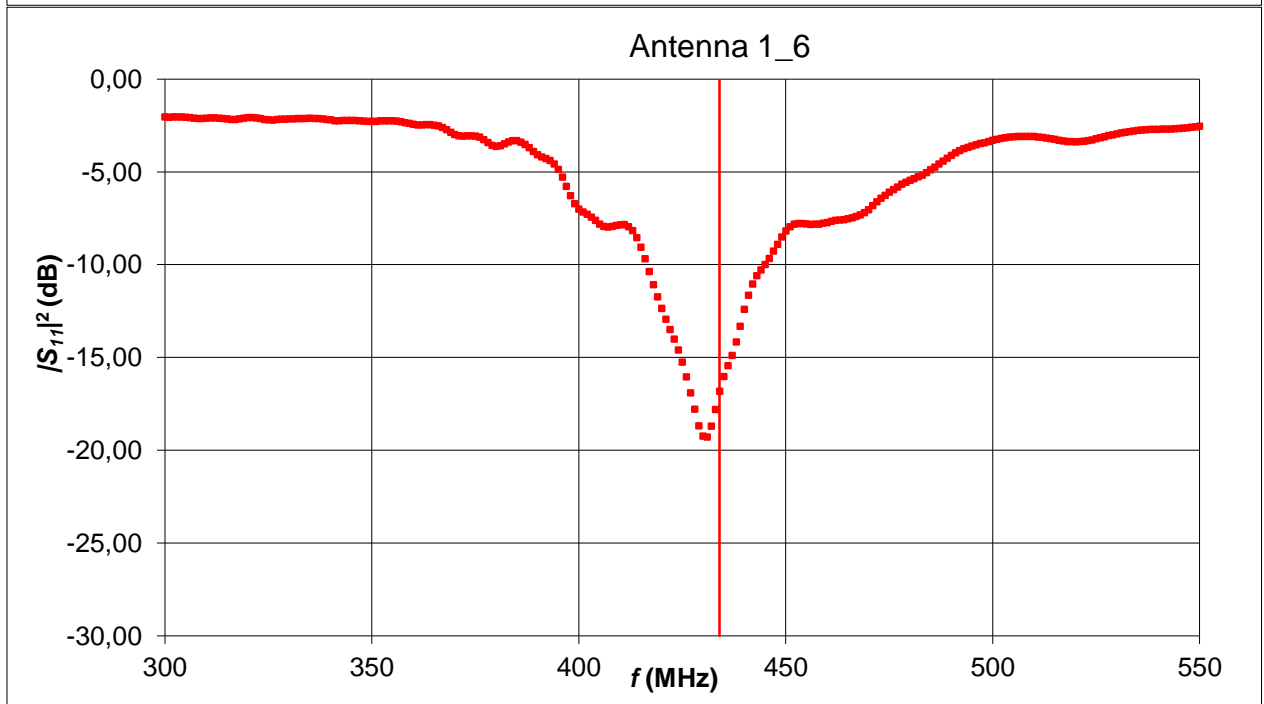
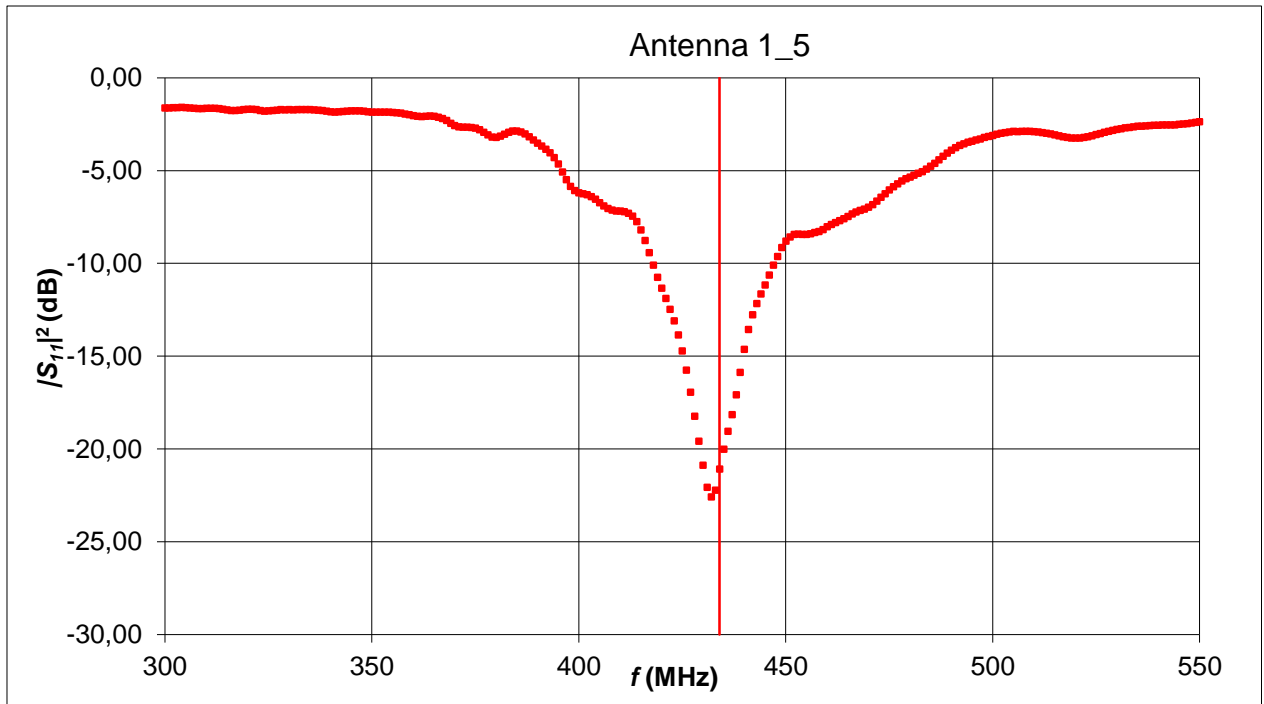
Figure A.2; the measurement setup for the power measurements.

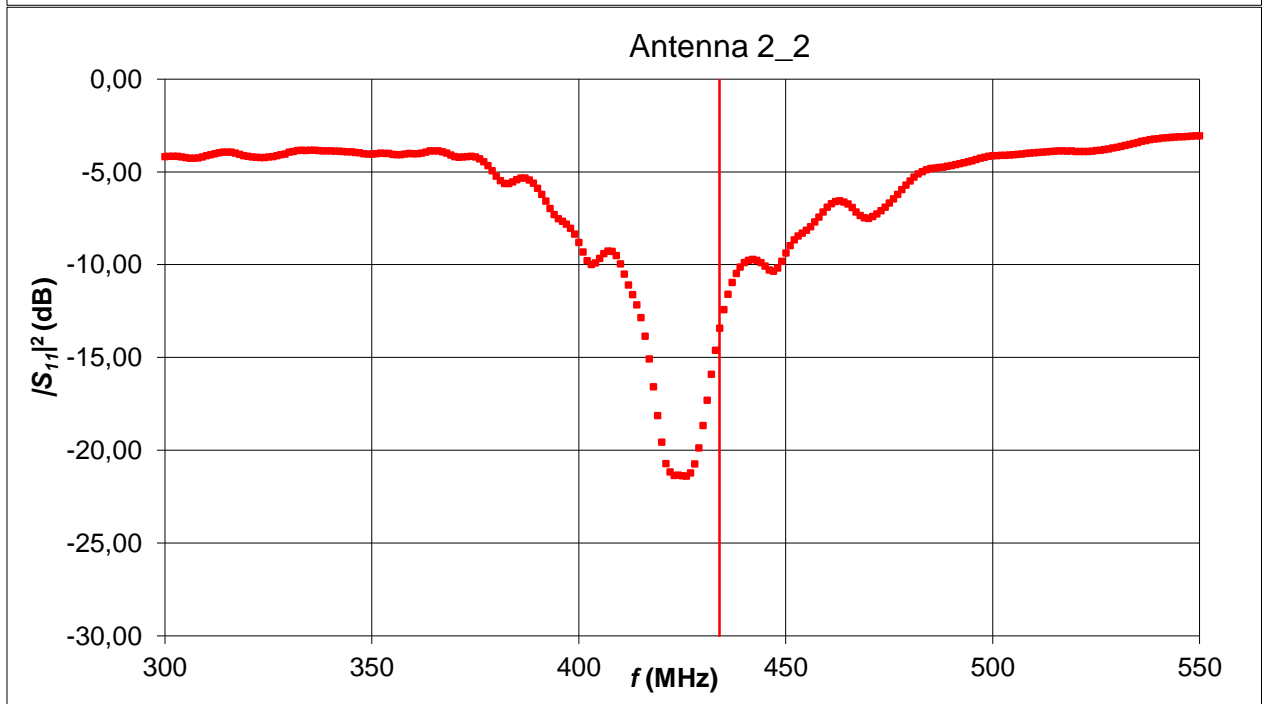
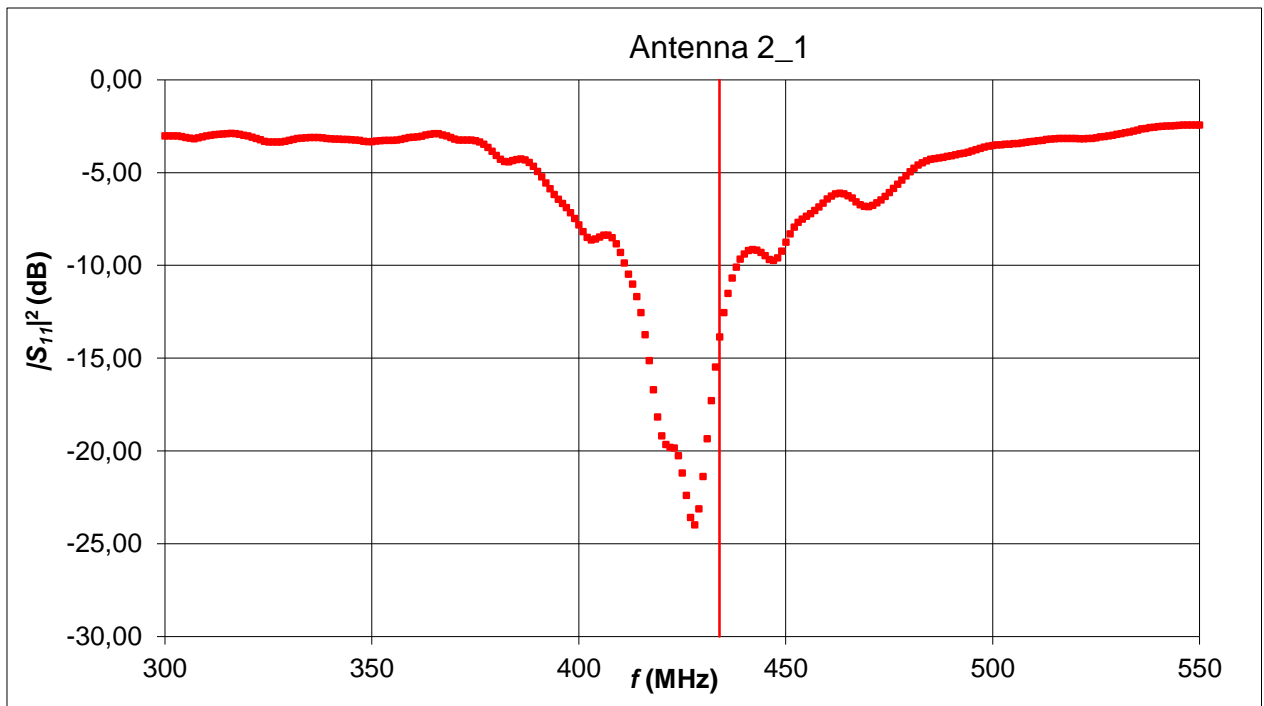
## Appendix IV: Results

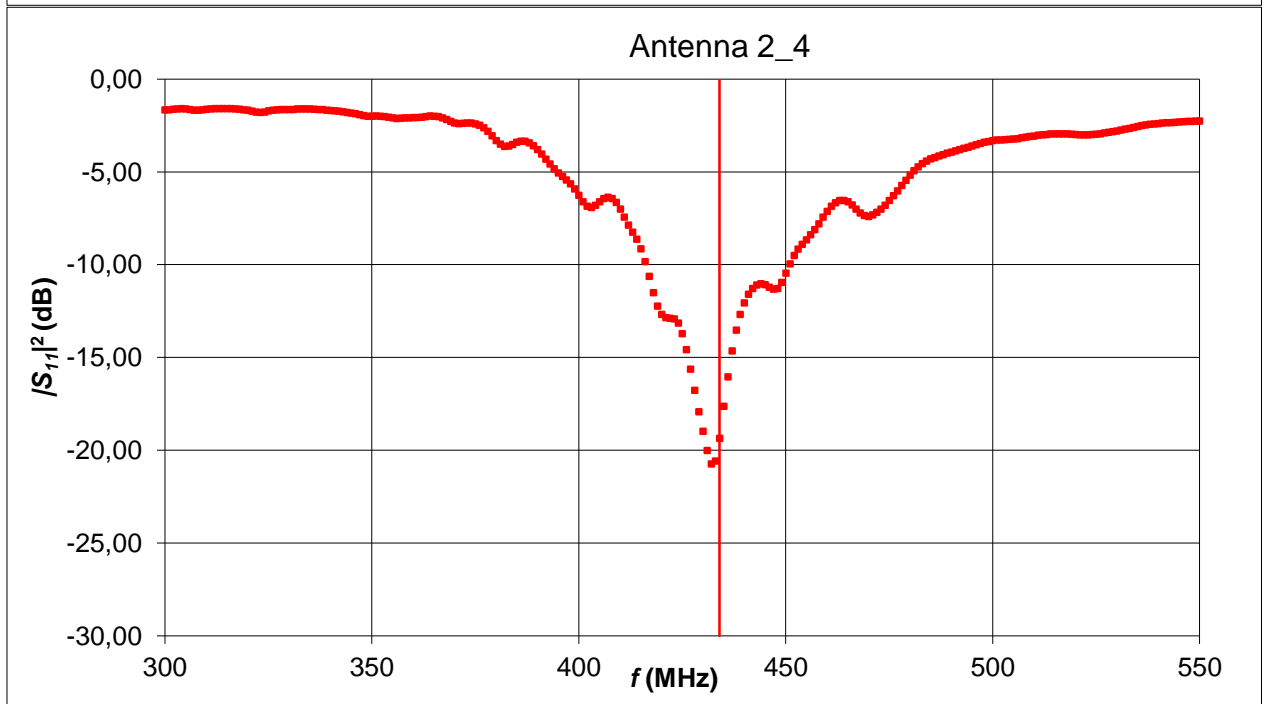
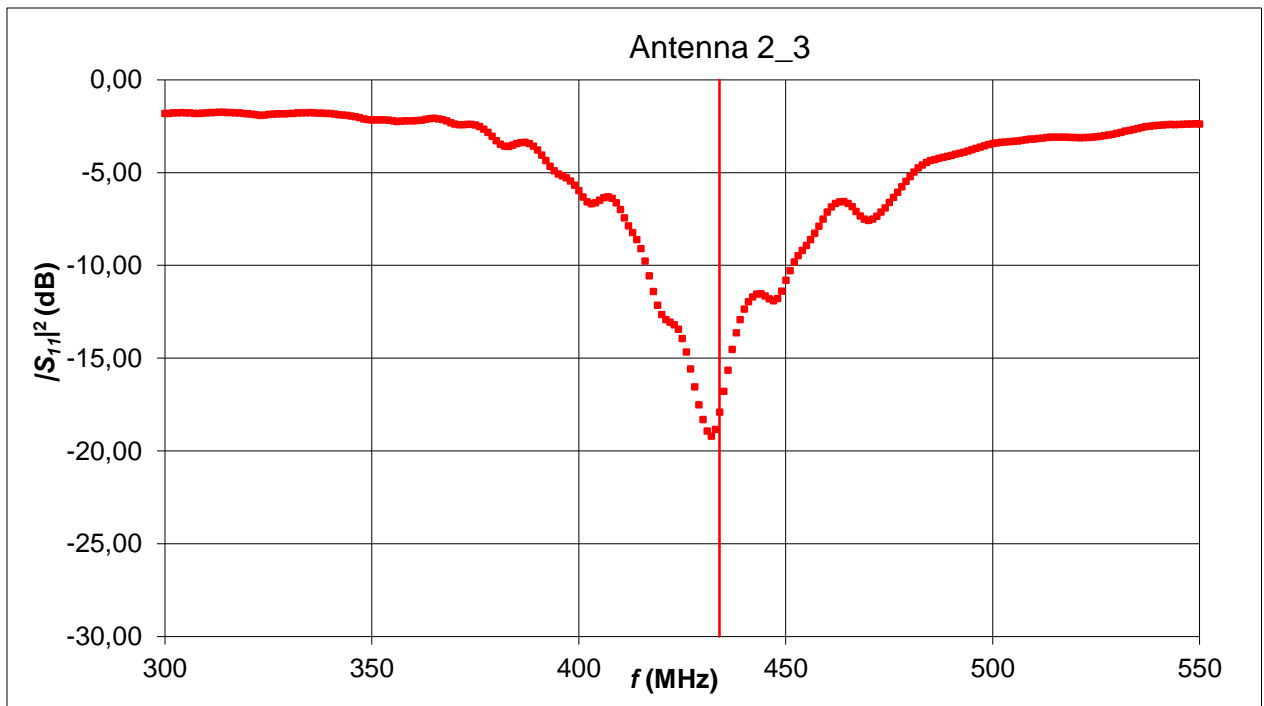
### $S_{11}$ measurements

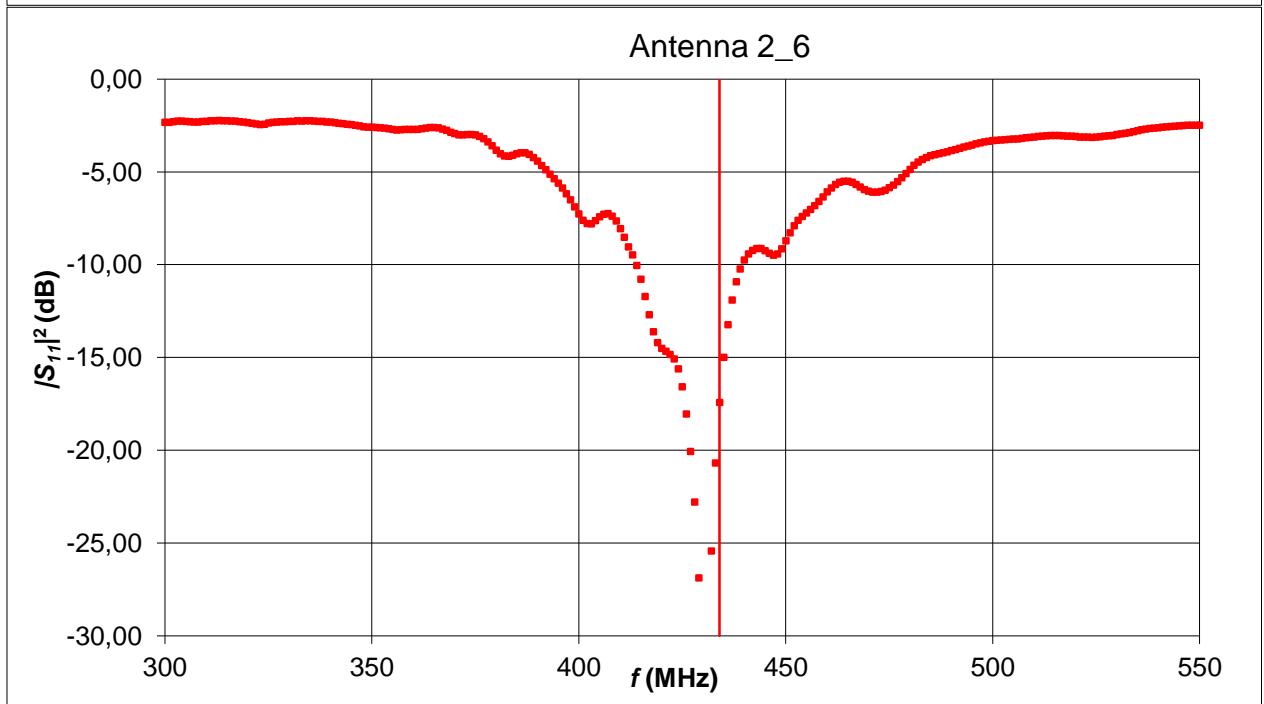
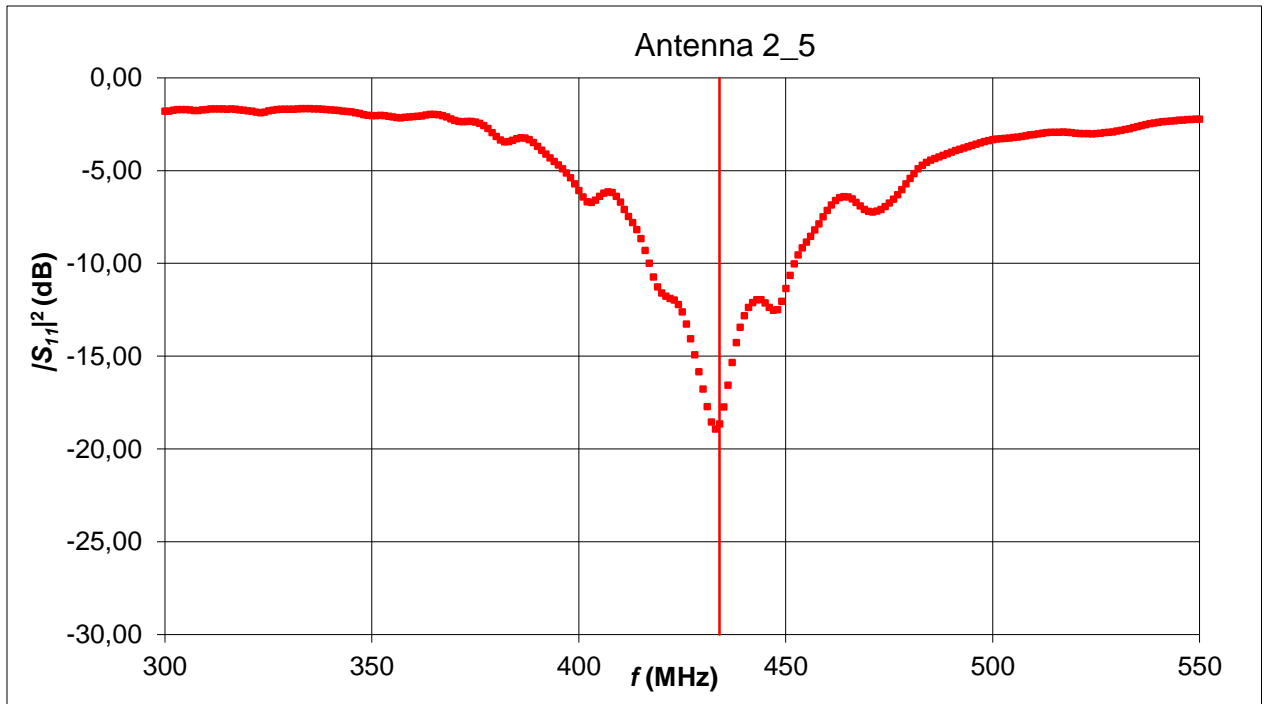




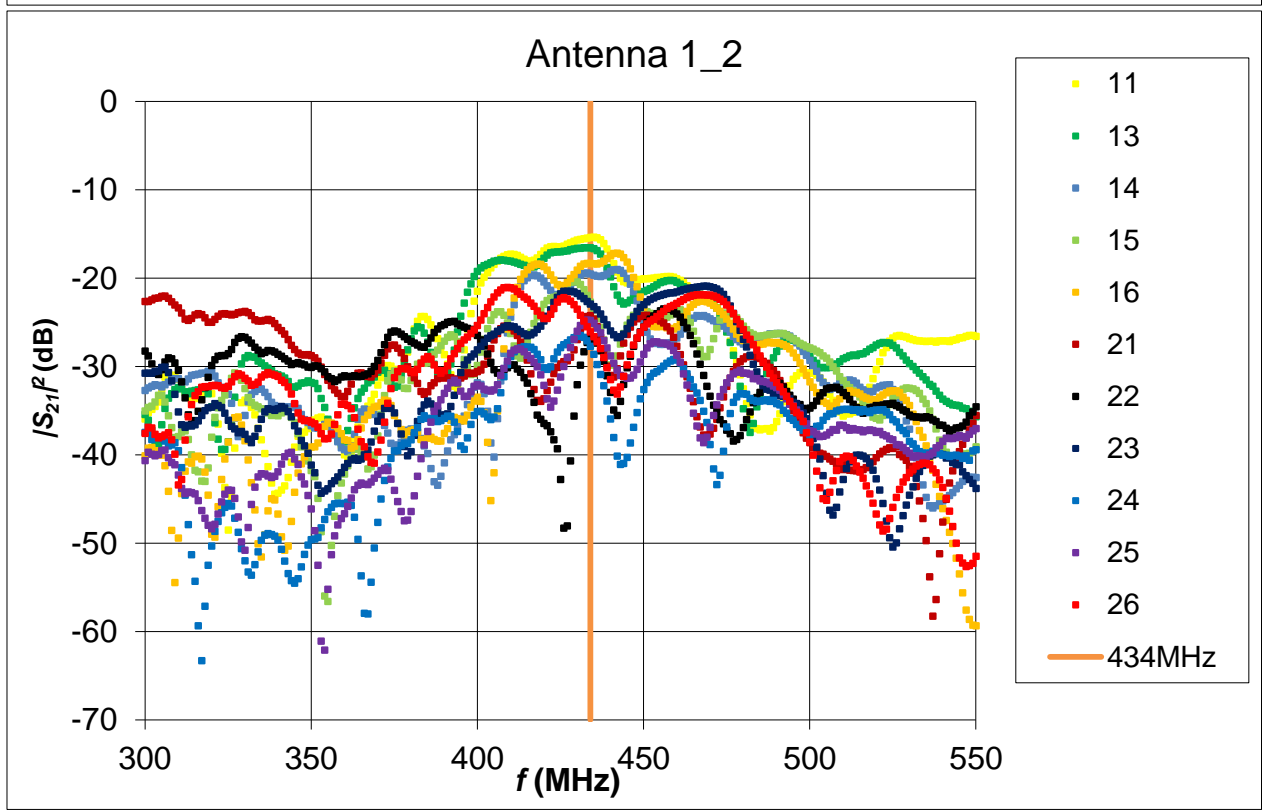
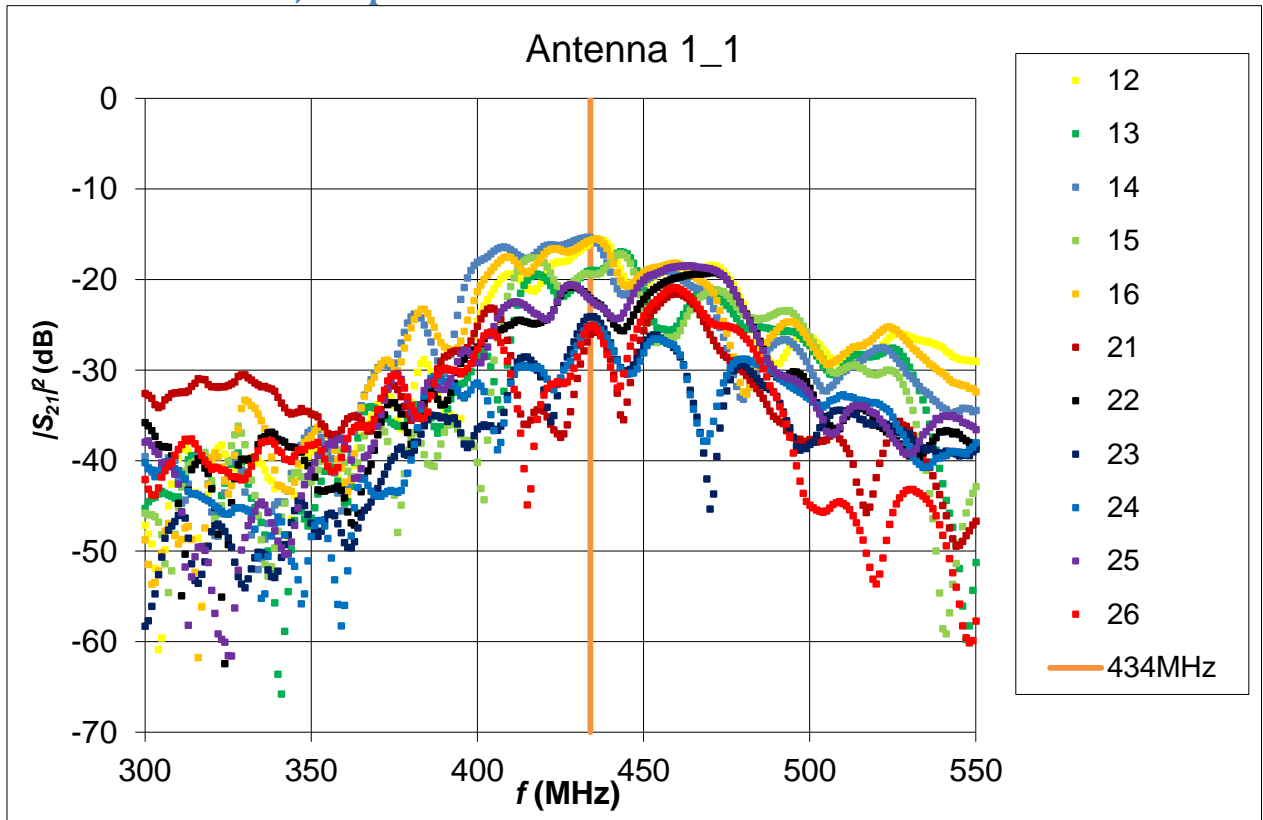


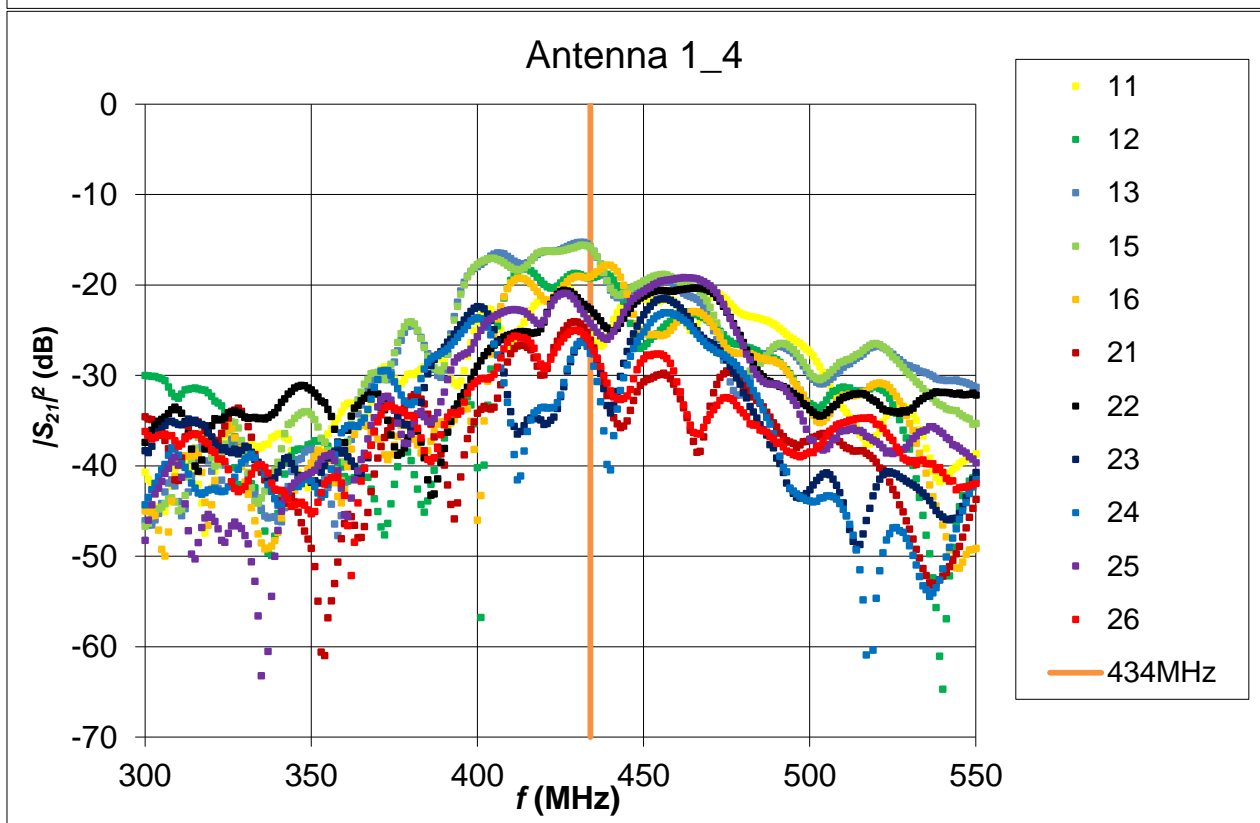
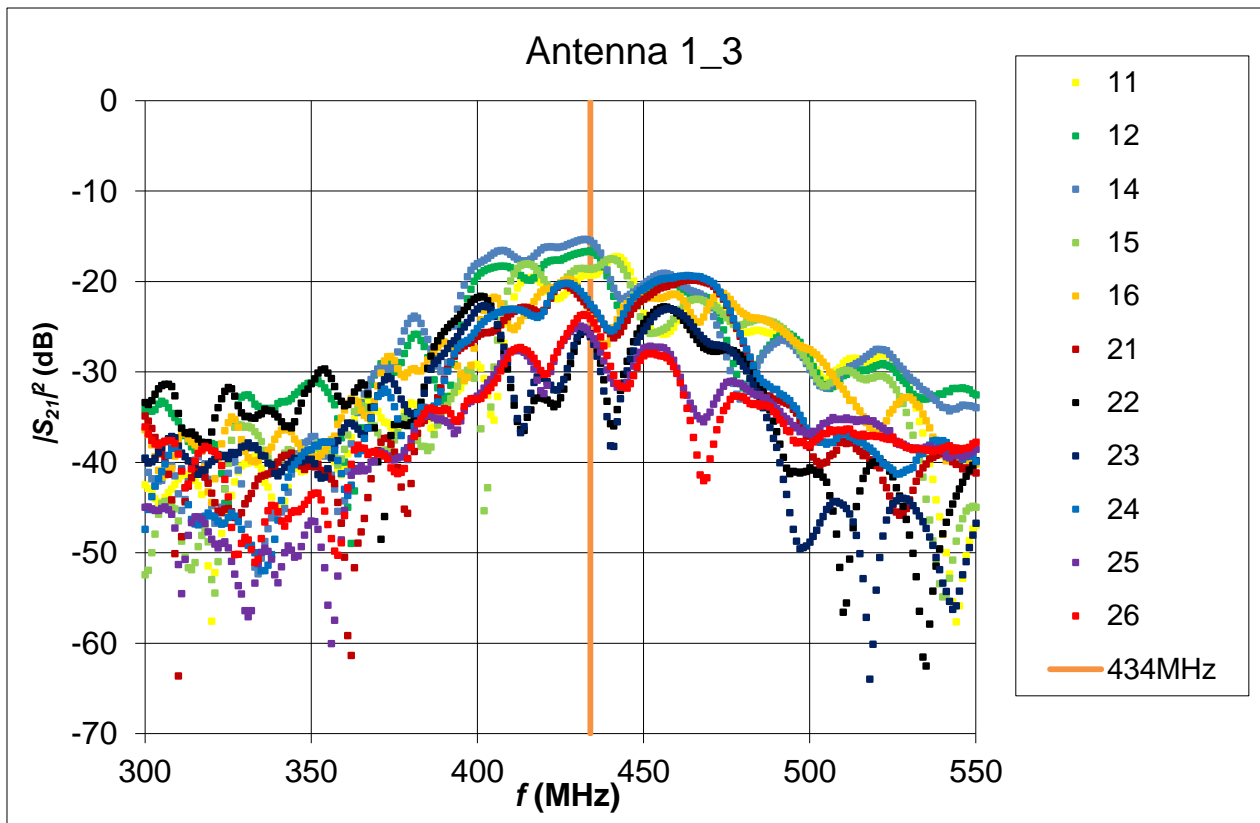


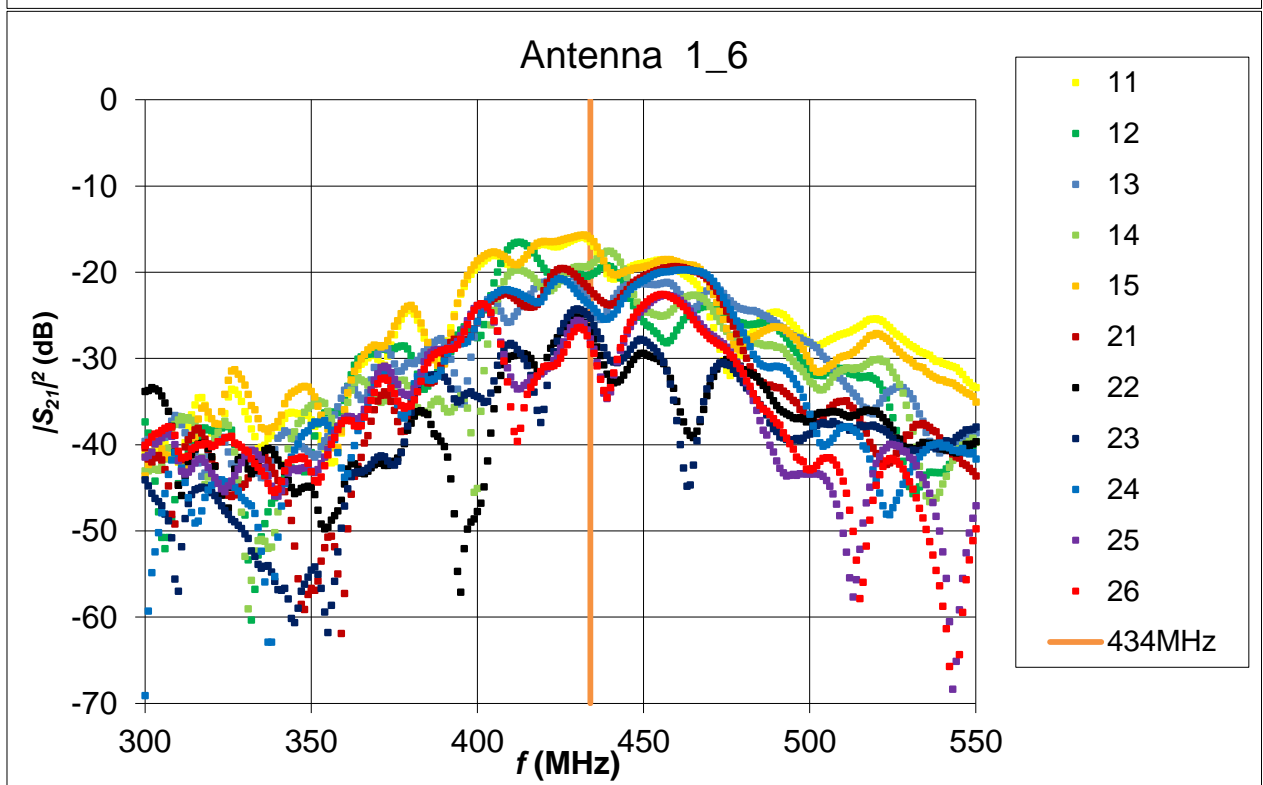
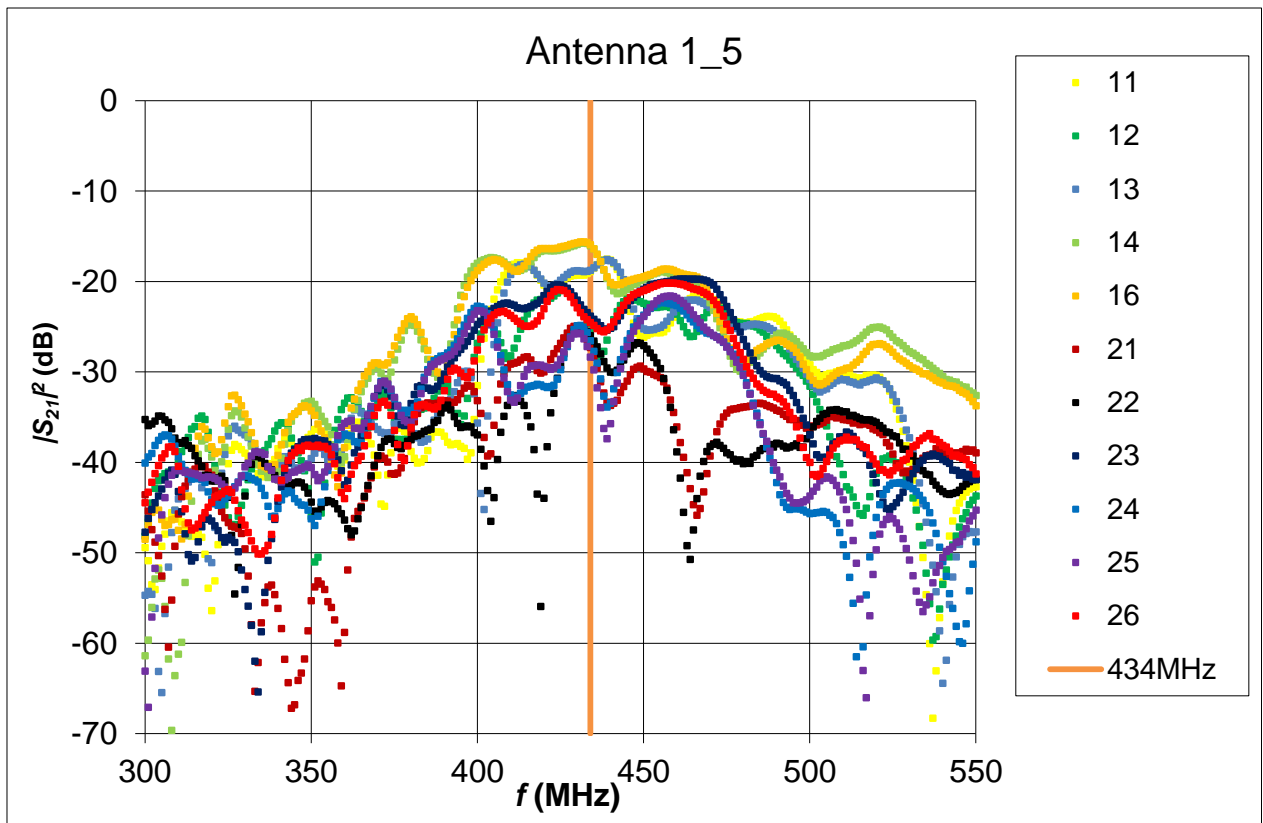


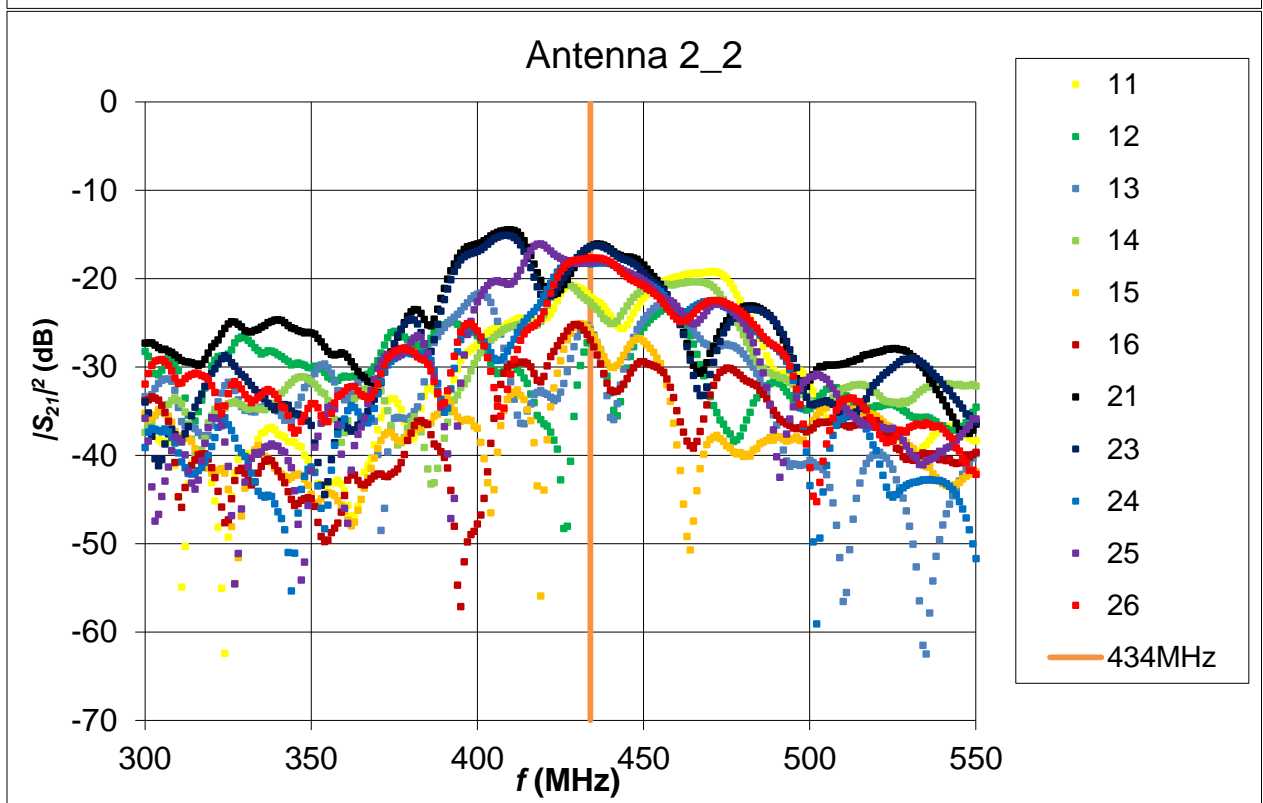
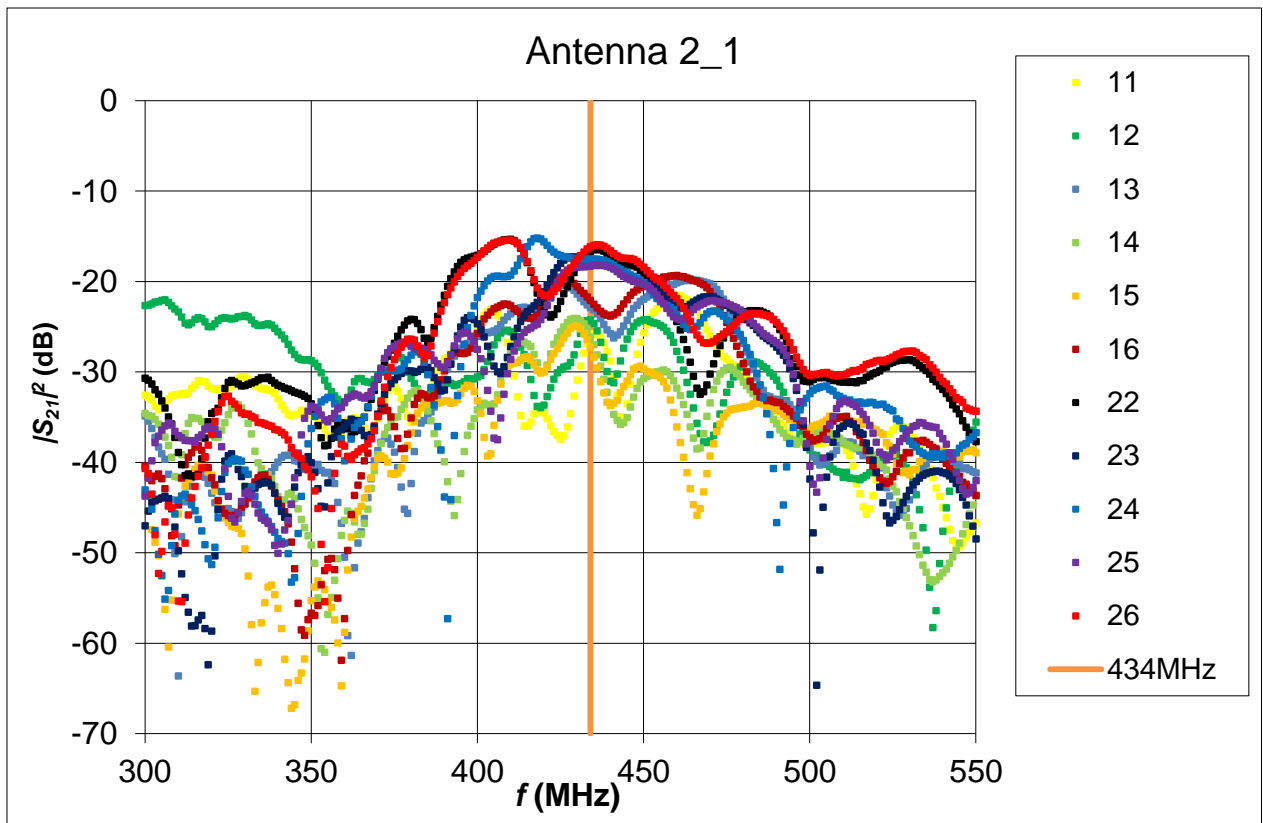


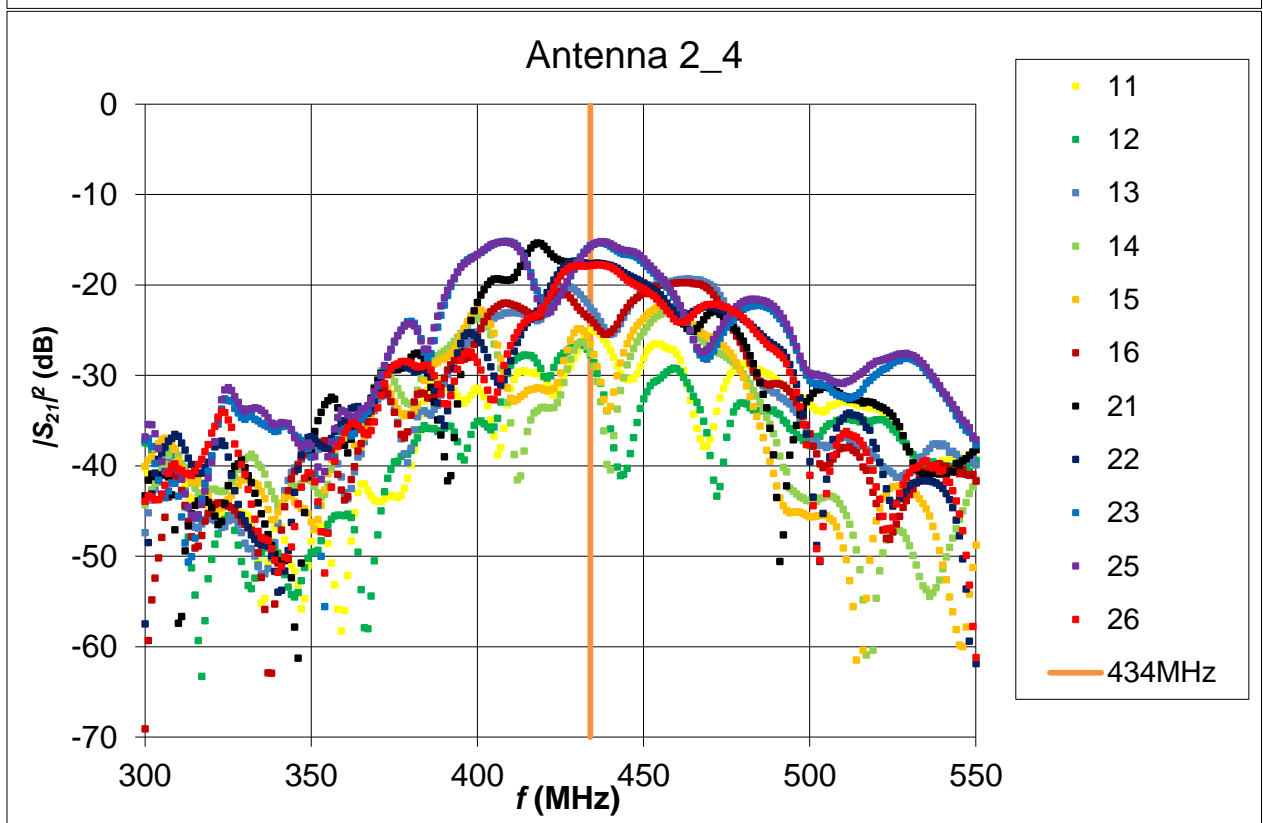
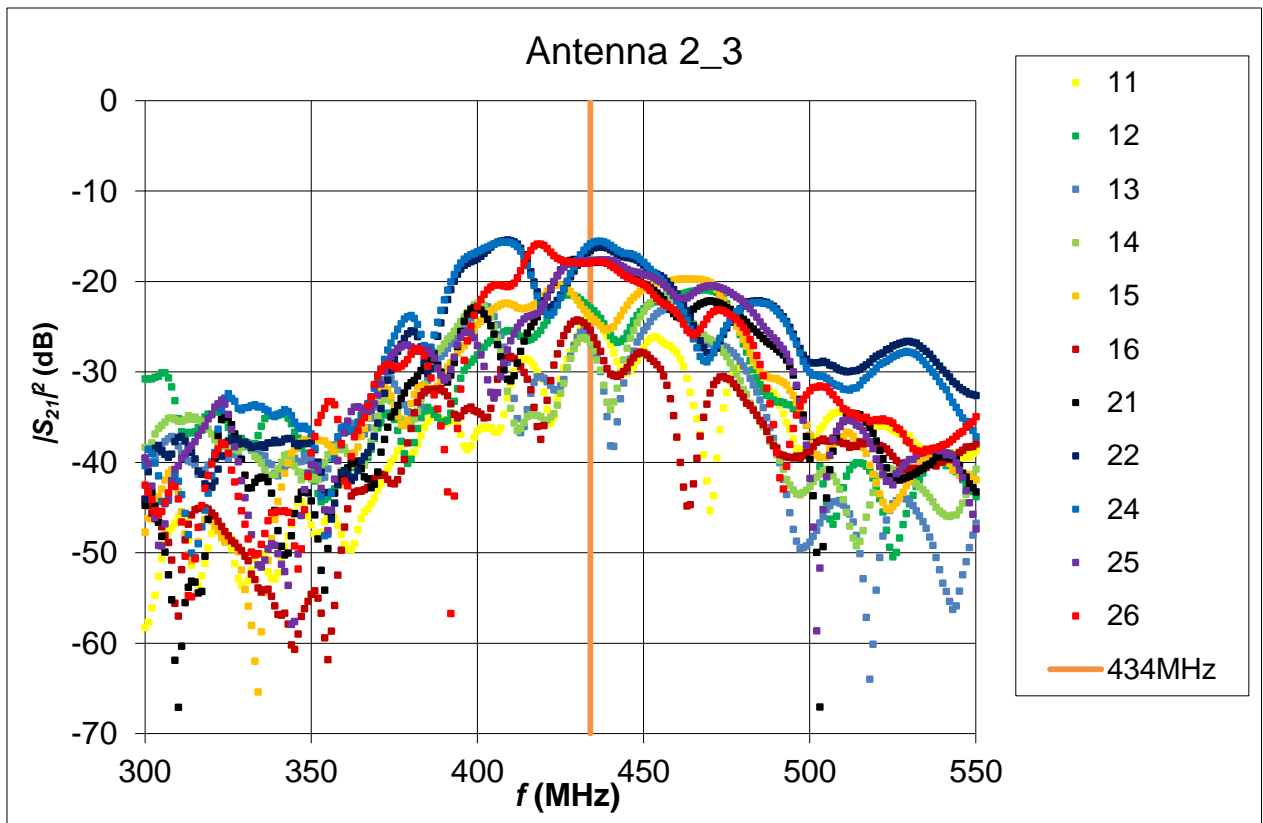
### S<sub>21</sub> measurements, Graphs

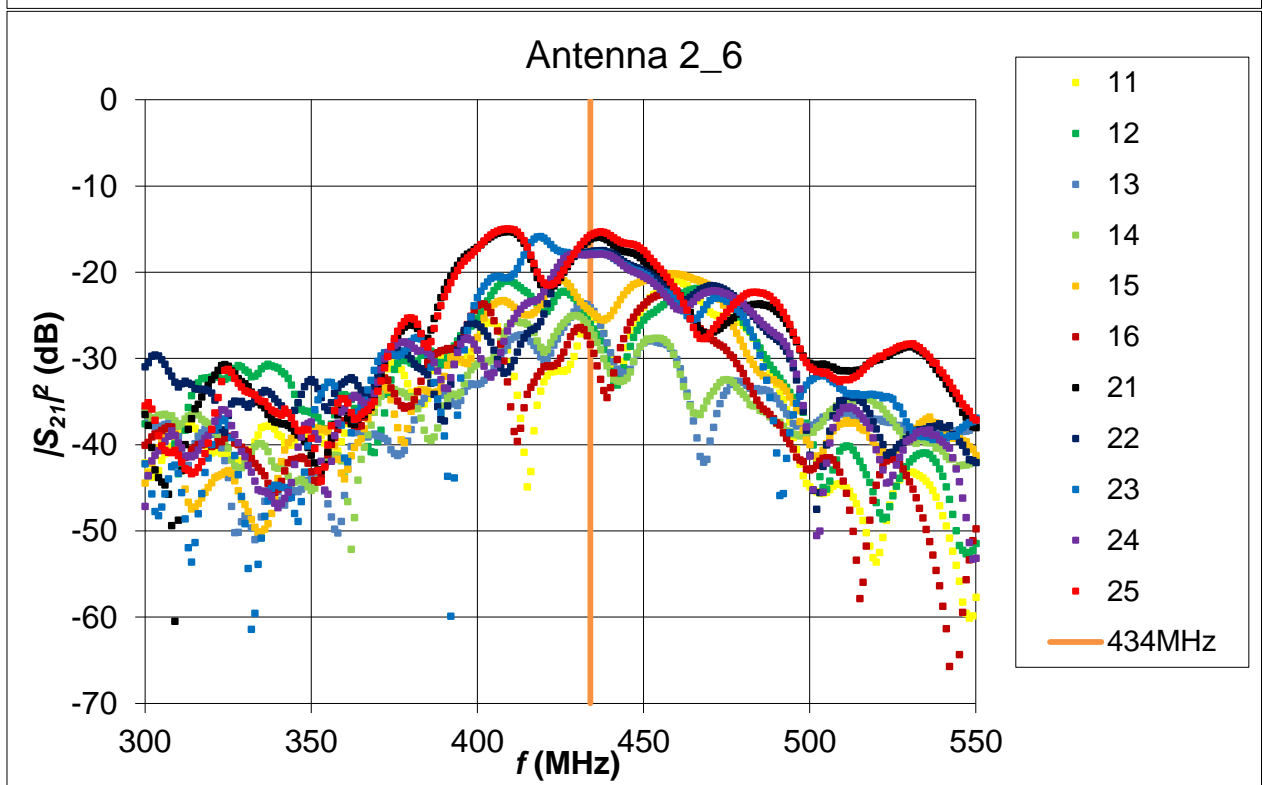
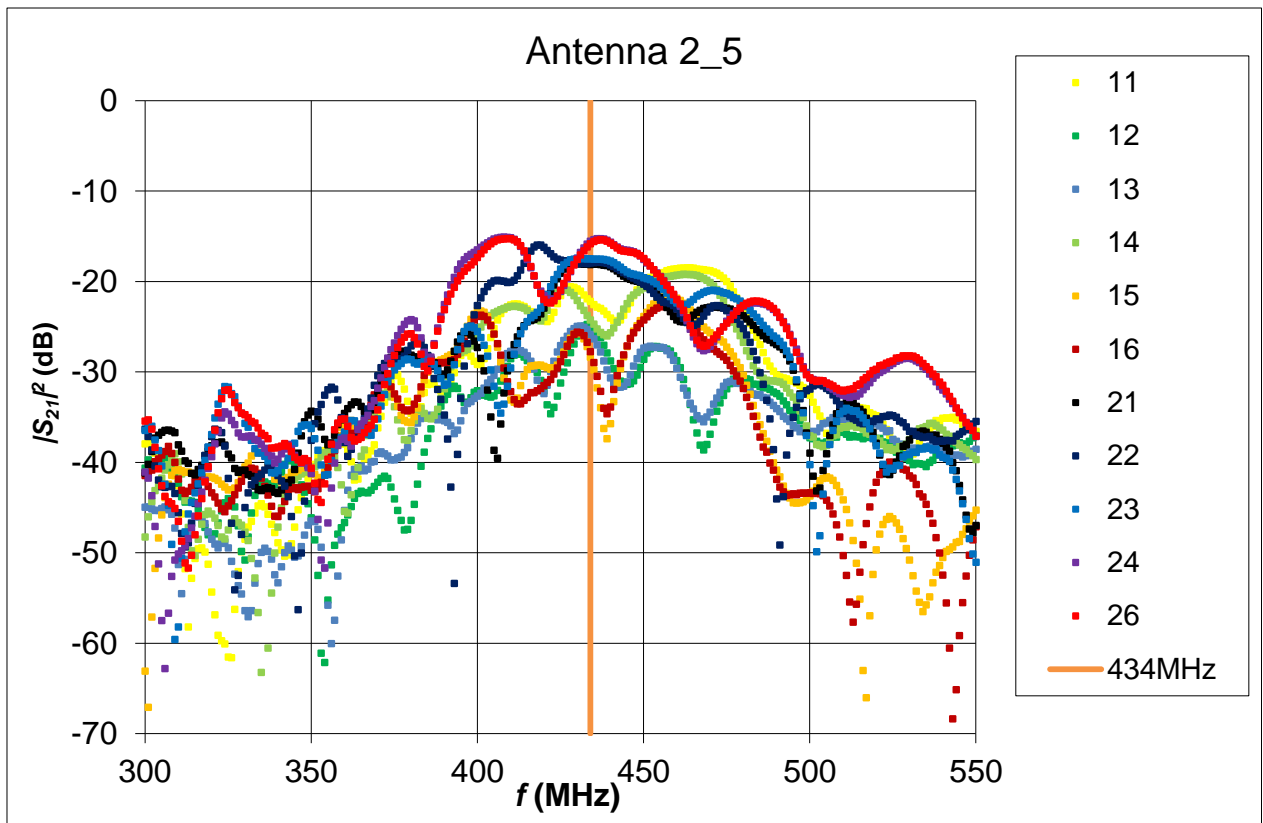






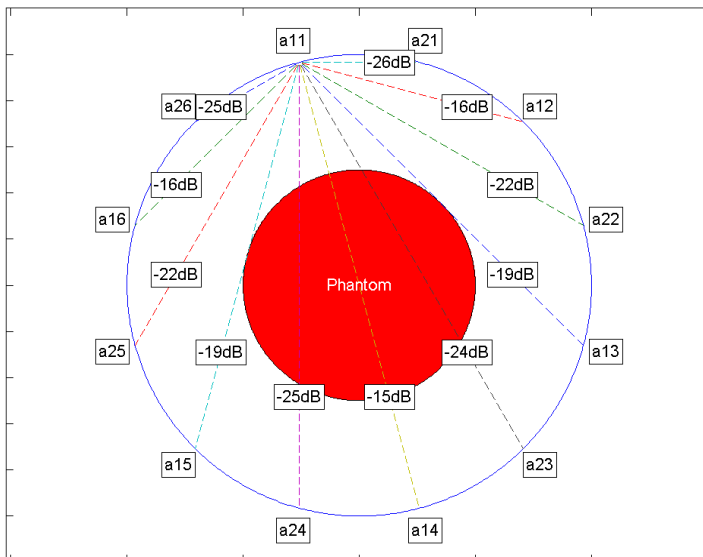




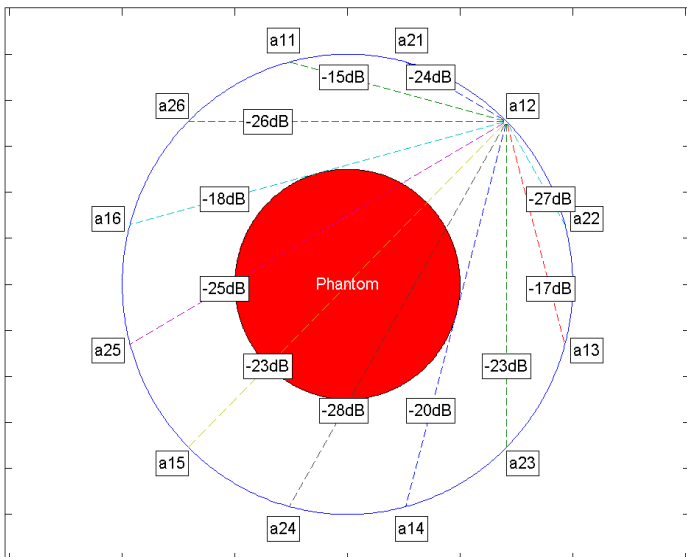


# $S_{21}$ measurements, values at 434 MHz

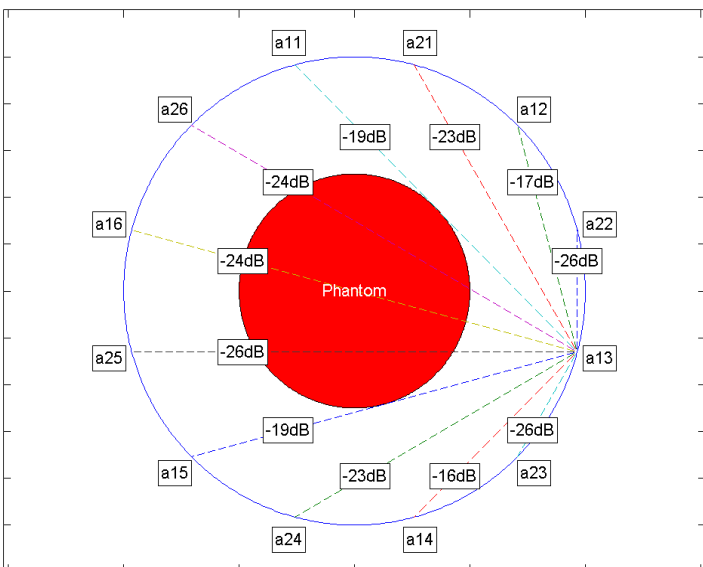
$|S_{21}|^2$  for antenna 1\_1 at 434 MHz (T = 27° C)



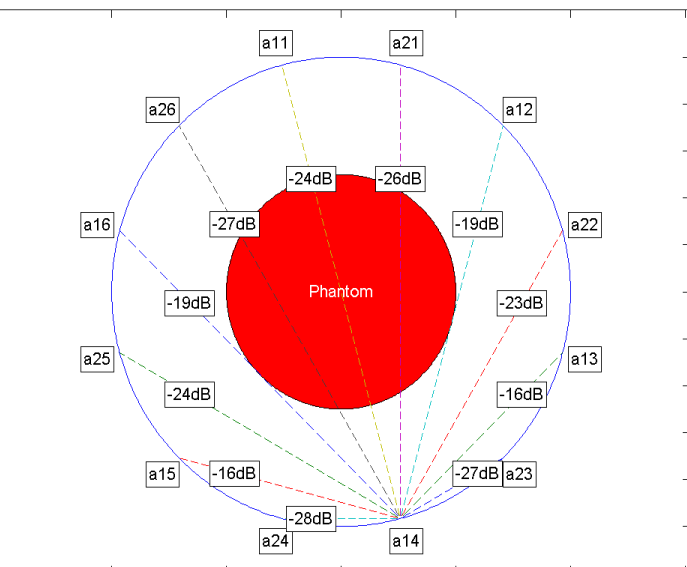
$|S_{21}|^2$  for antenna 1\_2 at 434 MHz (T = 27° C)



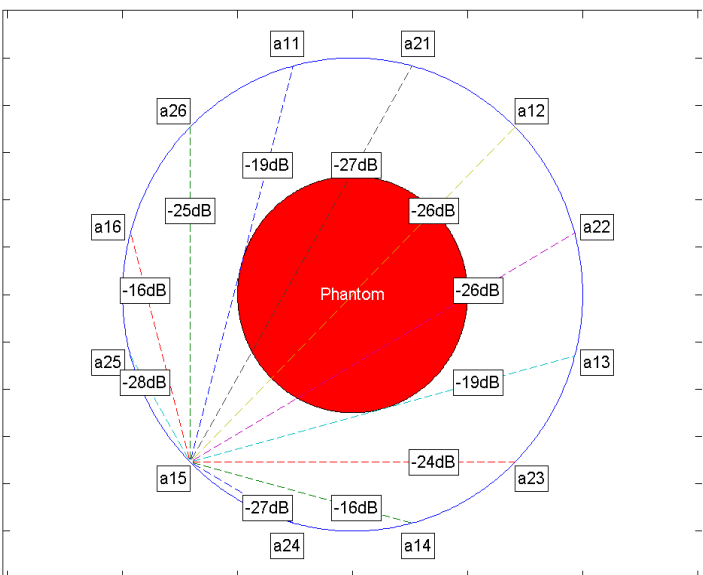
$|S_{21}|^2$  for antenna 1\_3 at 434 MHz (T = 27° C)



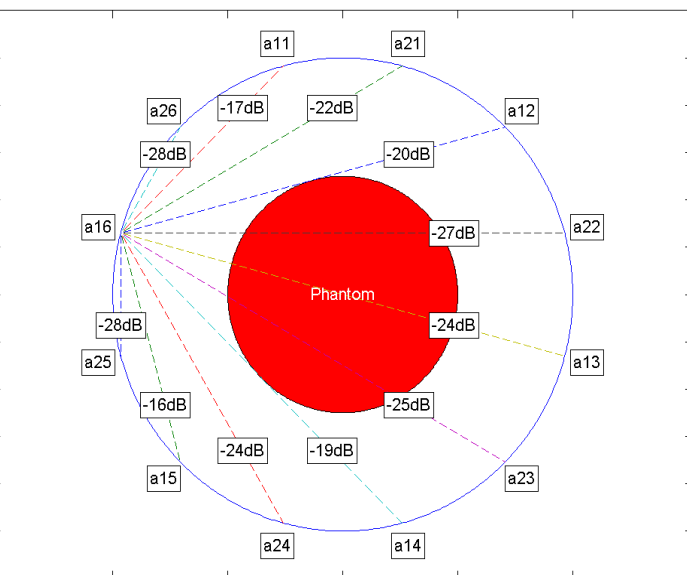
$|S_{21}|^2$  for antenna 1\_4 at 434 MHz (T = 27° C)



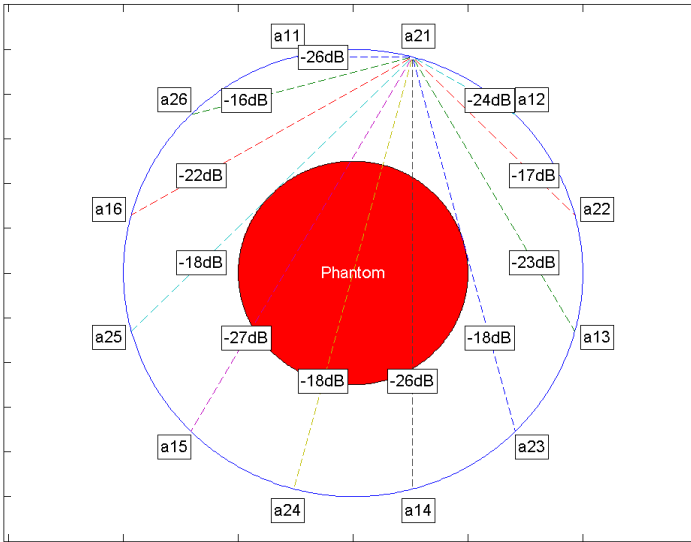
$|S_{21}|^2$  for antenna 1\_5 at 434 MHz (T = 27° C)



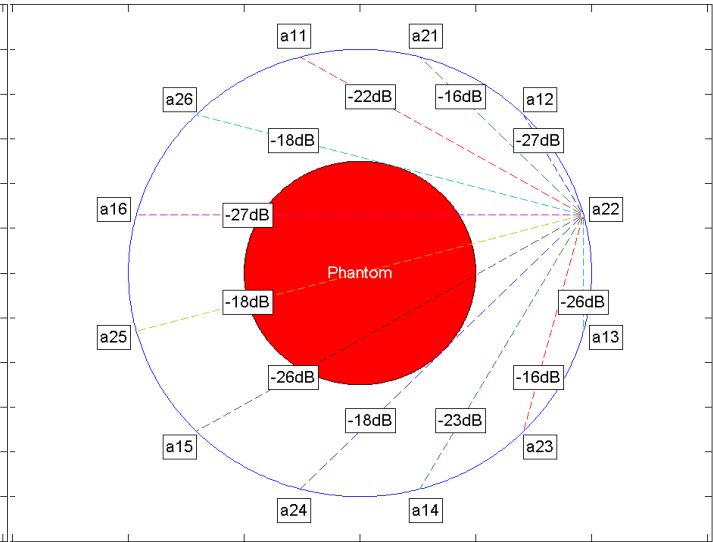
$|S_{21}|^2$  for antenna 1\_6 at 434 MHz (T = 27° C)



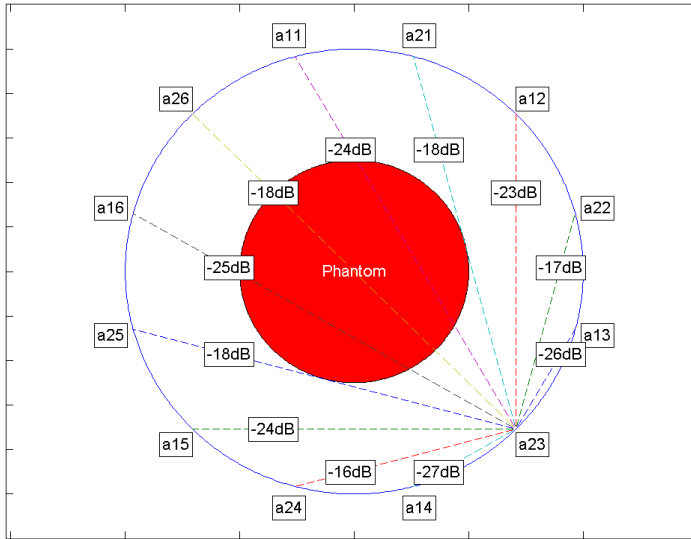
$|S_{21}|^2$  for antenna 2\_1 at 434 MHz (T = 27° C)



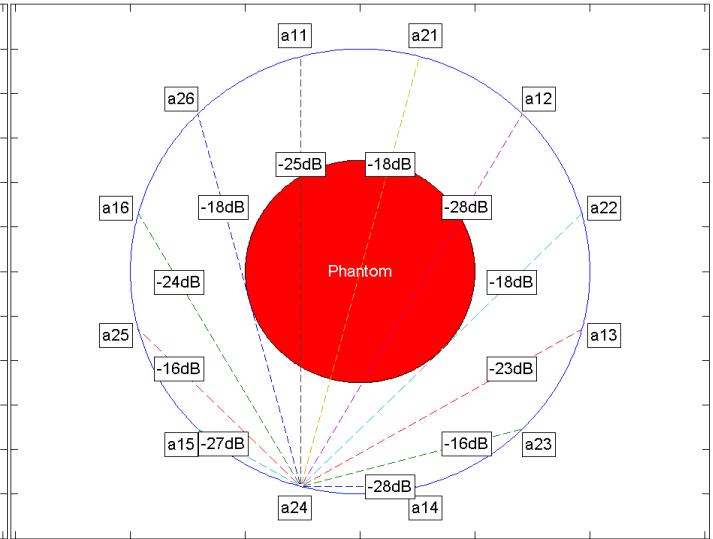
$|S_{21}|^2$  for antenna 2\_2 at 434 MHz (T = 27° C)



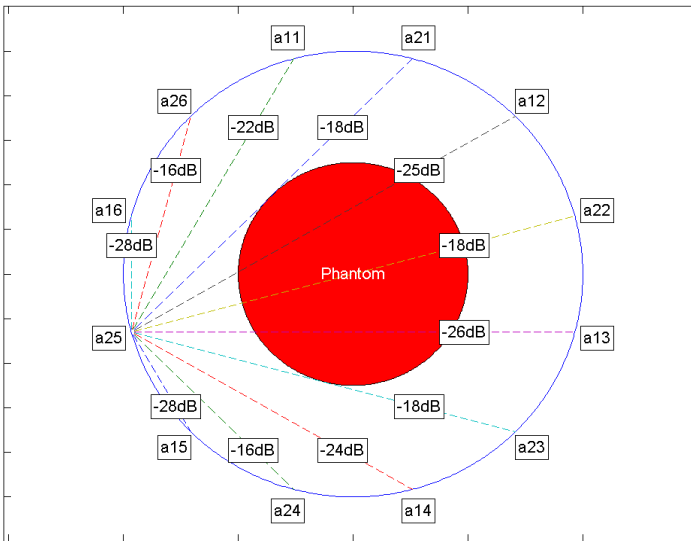
$|S_{21}|^2$  for antenna 2\_3 at 434 MHz (T = 27° C)



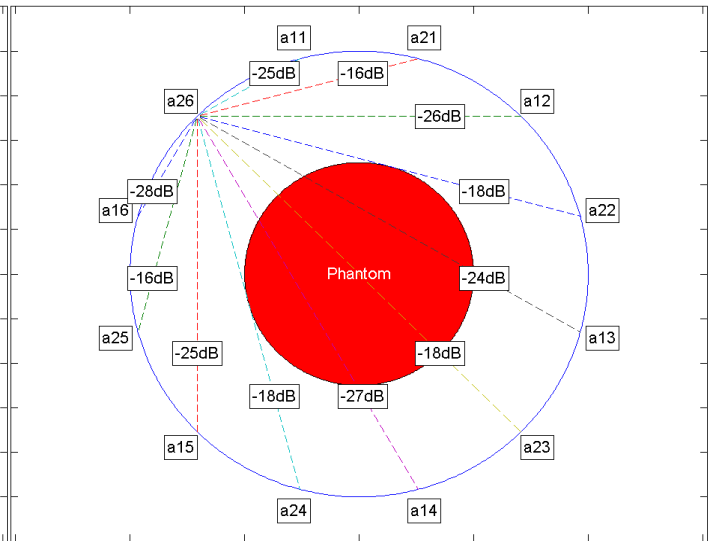
$|S_{21}|^2$  for antenna 2\_4 at 434 MHz (T = 27° C)



$|S_{21}|^2$  for antenna 2\_5 at 434 MHz (T = 27° C)



$|S_{21}|^2$  for antenna 2\_6 at 434 MHz (T = 27° C)



## Antenna 1\_2

To test the effect of moving the cable on the reflection of the antennae, two measurement sets were done. For antenna 1\_2 and 1\_3, nine  $S_{11}$  measurements were performed while after each measurement the coax cable, which connects the antenna to the VNA, was moved. The cable was moved the same way for antenna 1\_2 and 1\_3. The water temperature during the measurement was stable at  $22 \pm 1$  °C. Figure A.3 and A.4 show the  $RL$  coefficients for antenna 1\_2 and 1\_3 respectively. They clearly show that antenna 1\_2 is affected by the movement of the cable, while antenna 1\_3 shows no significant response.

At 434 MHz, the  $RL$  varies between -5.78 and -8.81dB. Keep in mind that we showed that for higher temperatures, the  $f_{res}$  increases, which means that for these temperatures the  $RL$  variance increases. At 22 °C, the highest measured change in  $RL$  is at 414 MHz, where the  $RL$  varies between -9.8 and -33.4dB. For antenna 1\_3, at 434 MHz the  $RL$  varies between -13.2 and -13.8dB, while at the  $f_{res}$  (426 MHz) the values go from -25.0 to -28.0.

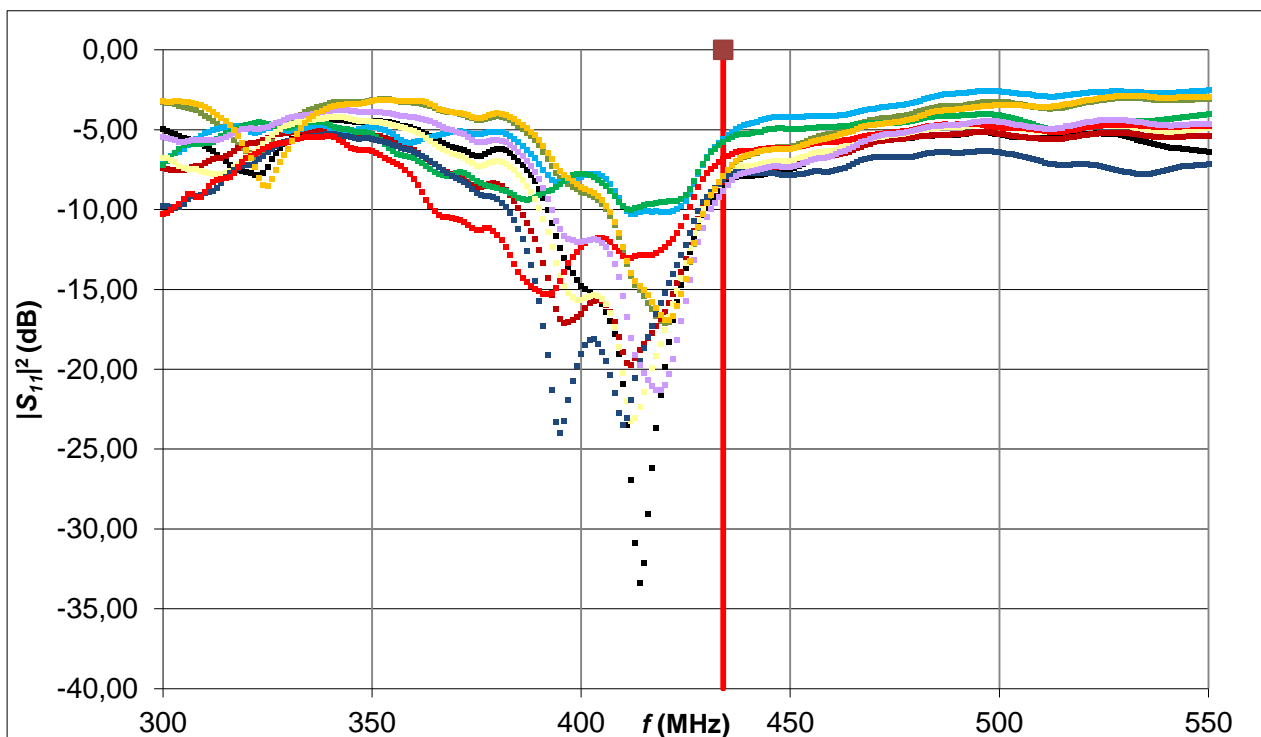


Figure A.3; the measured  $RL$  for antenna 1\_2 while moving the cable it is attached to. A total of nine measurements was performed.

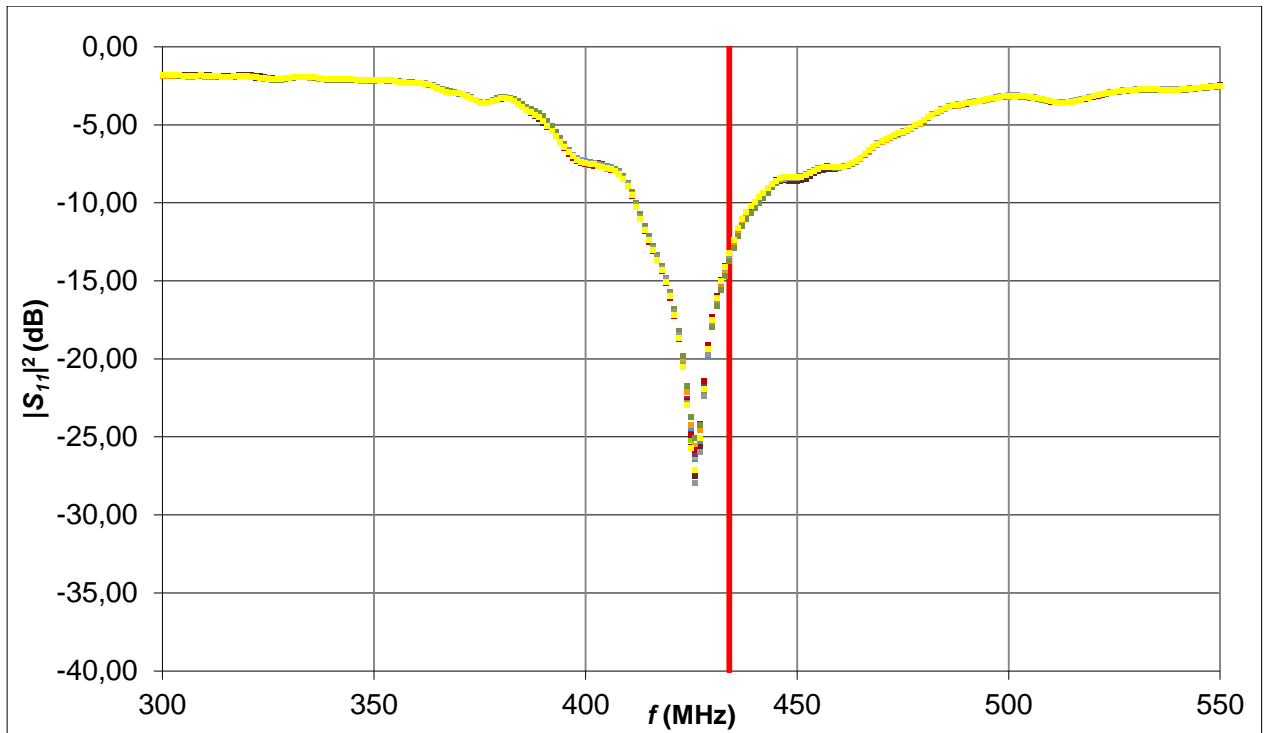
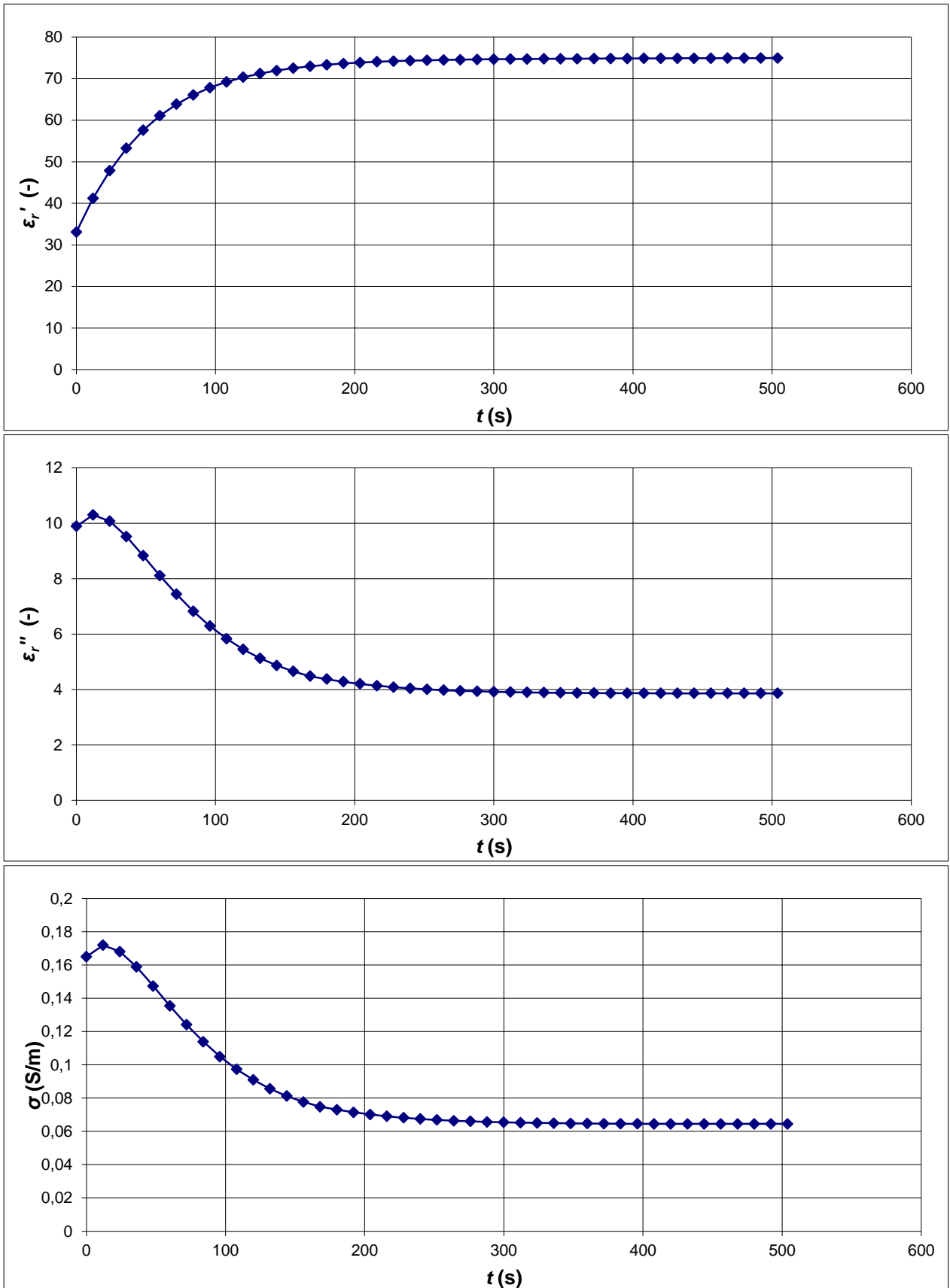


Figure A.4; the measured RL for antenna 1\_3 while moving the cable it is attached to. A total of nine measurements was performed.

## Time dependency of the dielectric measurement kit and the VNA

The following figure shows the measurement of the dielectric properties of demineralised water using the dielectric measurement kit and the VNA. It shows that it takes time to measure the correct value.



## **Appendix V: The original assignment**

In de Daniel den Hoed kliniek is de MRlabcollar gebouwd. Dit apparaat is een experimentele hyperthermie opstelling die door de afwezigheid van Ferromagnetische materialen in de MRI gebruikt kan worden. Het doel is het karakteriseren van de antennes die in de MRlabcollar zijn ingebouwd, door het doen van onder andere warmte, en S-parameter metingen. Ook zal een fantoom gebouwd worden, gebaseerd op eigenschappen van het menselijk lichaam. Dit om de metingen zo reëel mogelijk te laten verlopen.

A MRlabcollar applicator has been designed and constructed. This device is an experimental hyperthermia setup that can, due to the absence of Ferromagnetic materials, be used inside the MRI. The goal is the characterisation of the antennae which are built into the MRlabcollar, by doing measurements including temperature, and S-parameters. Furthermore, a phantom will be fabricated, based on human tissue properties, so that the measurements will be as valid as possible.